Hierarchical nanomaterials by selective deposition of noble metal nanoparticles: Insight into control and growth processes

Oleg Baranov, Thierry Belmonte, Igor Levchenko, Kateryna Bazaka, Martin Košiček, Uroš Cvelbar

Revised version (adts.202300288)

Hierarchical nanomaterials by selective deposition of noble metal nanoparticles: Insight into control and growth processes

Oleg Baranov[1,2], Thierry Belmonte[3], Igor Levchenko[4,5], Kateryna Bazaka[4], Martin Košiček[2,6] and Uroš Cvelbar[2,6*]*

[1] *Plasma Laboratory, National Aerospace University, Kharkiv, Ukraine*
[2] *Department of Gaseous Electronics, Jozef Stefan Institute, Ljubljana 1000, Slovenia (EU).*
[3] *Université de Lorraine, CNRS, IJL, F-54000 Nancy, France (EU)*
[4] *School of Engineering, College of Engineering, Computing and Cybernetics, The Australian National University, Canberra, ACT 2600*
[5] *Plasma Sources and Application Center, NIE, Nanyang Technological University, Singapore 639798*
[6] *Jožef Stefan International Postgraduate School, Ljubljana, Slovenia (EU)*
*Corresponding author email: O.Baranov@khai.edu and uros.cvelbar@ijs.si

Complex hierarchical metamaterials are currently the focus of many cutting-edge studies due to their potential to advance such critically important areas of technology as energy storage and transformation, sensing, photovoltaics, nano-medicine, antibacterial and self-regenerating materials. However, deterministic design of novel hierarchical metamaterials remains problematic due to the lack of efficient, highly reliable methods for controlling the internal structure and design of materials. Here we propose an advanced comprehensive model to simulate the formation of complex hierarchical metamaterials with controllable structure. The control is achieved via selective deposition of noble metal nanoparticles (Au, Au, Pd, Pt). Moreover, we theoretically examine and experimentally verify the novel method. This approach allows for the sophisticated spatiotemporal control of growth conditions and, as a result, achieving the targeted internal structure of metamaterials. This opens a way to the deterministic design and formation of complex multi-material metamaterials on the basis of metal oxides and noble metal nanoparticles. Moreover, we present a fundamental insight related to the longstanding question about the bottom-up and top-down growth types that vary for various materials and systems, and is quite difficult for the direct experimental verification.

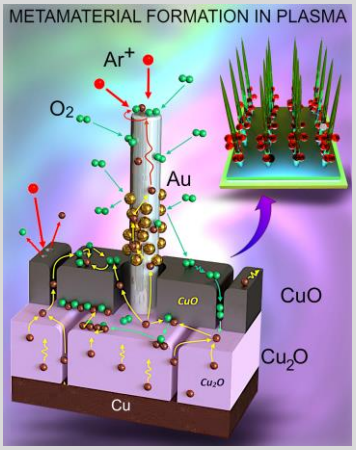

1. Introduction

Complex hierarchical nanomaterials and metamaterials are currently in the focus of research efforts worldwide.[1,2,3] Multicomponent architectures at nanoscale feature many unique properties and functions, which enable various applications including biological,[4] gas and mechanical sensors,[5,6] devices for energy collection and storage,[7,8,9] nanoscale therapeutic systems,[10,11] platforms for light-driven[12] and chemical catalytic reactions,[13,14] biotechnological applications,[15,16] hydrogen fuel production,[17] wastewater decontamination,[18] and technologies for space exploration and space economy.[19-22] However, the trial and error approach which is often used for designing the hierarchical metamaterials is limited for its high cost. Besides, it is slow and does not guarantee the desired results. Here we propose, theoretically examine via advanced simulations, and then experimentally verify a new approach for the deterministic assembly of complex nanomaterials. In this approach, selective deposition of metal nanoparticles is used to sophisticatedly control the formation of the desired internal structure.

As a model system we have selected the hierarchical metamaterial primarily consisting of long metal oxide (CuO) nanowires loaded with noble metal (gold) nanoparticles. Such systems are promising due to their outstanding morphology-conditioned properties.[23] Among other metal oxide nanowires, arrays of copper oxide nanowires exhibit excellent properties required for advanced batteries,[24] field emission devices,[25] and supercapacitor applications.[26,27] However, copper oxide-based metamaterials suffer from such shortcomings as e.g. high rates of agglomeration, low conductivity and electrochemical stability. These could be overcome by synergistically combining CuO with e.g. conducting polymers, carbon nanotubes or graphene-based materials[28,29] using *in situ* modification of copper foam,[30] room temperature chemical synthesis,[31] high temperature annealing,[32] thermal oxidation of pre-synthesized copper nanowires,[33] facile solution-phase technique,[34] anodization in sodium bicarbonate solution,[35] thermal oxidation of copper foil in oxygen[36] and many other methods.[37]

Such a plethora of available technologies naturally resulted in many studies aimed to reveal the parameters that control the growth, with the central question: - *Is it possible to efficiently control the architecture, structure, and morphology of the growing material through the simple adjustment of the synthesis conditions?* Experiments that varied temperature,[38] heating rate,[39] oxygen flow,[40] humidity and external electric field,[41] initial roughness of copper substrates[42] and others have demonstrated these parameters cannot definitively control the growth. Besides, near all of above-mentioned parameters are inter-dependent and not always could be directly controlled – e.g. substrate roughness affects surface growth via diffusion, yet itself can change during the process due to sputtering; strong electric fields could be generated at long nanowires due to charging,[43] and so on. Based on this, we can state:

- ✓ *It is unlikely that complex hierarchical metamaterials could be deterministically assembled using a relatively simple control sequence of direct controls such as temperature, time, gas pressure and similar*

This means that *some specialised control tools are needed for selective, deterministic control of the architecture, structure, and morphology of the growing hierarchical metamaterial.* In this article we demonstrate that (i) the method of selective deposition of nanoparticles is effective in controlling the morphology of the growing copper oxide nanoarrays, and (ii) this method is deterministic, i.e. the targeted structure can be predicted, modelled, and then synthesised. For this, we first modelled the whole growth under the selective deposition control that aimed to significantly enlarge the nanowires by re-distribution of diffusional fluxes using deposited nanoparticles, and then performed the direct experiment which demonstrated formation of targeted structures. Similar methods could be designed for material architectures that target specific applications, thus avoiding the *trial-end-error* method.

The discussed technological process includes three separate stages (**Figure 1**). At the first stage, an array of copper oxide nanowires on the substrate was formed by use of microwave atmospheric plasma discharge (until the nanowires cannot grow anymore) (i). Then, the deposition of gold nanoparticles on the array to cover the side surfaces of the nanowires by the noble metal (ii) was made. Finally, re-exposition of the modified array in the microwave plasma was used to increase the length of the nanowires (iii). This process was utilized by simulation and then by real physical synthesis. In this process, plasma is necessary to significantly accelerate the growth process, while the stage of the intermediate deposition of gold allows overcoming the limit of the maximal length of the nanowires conditioned by the limited diffusion path of copper from the nanowire root to the tip. Hence, the combination of the plasma-enhanced growth and the deposition of noble metals is utilized as a promising tool to synthesize the metal oxide nanowires in a productive and cost-effective way.

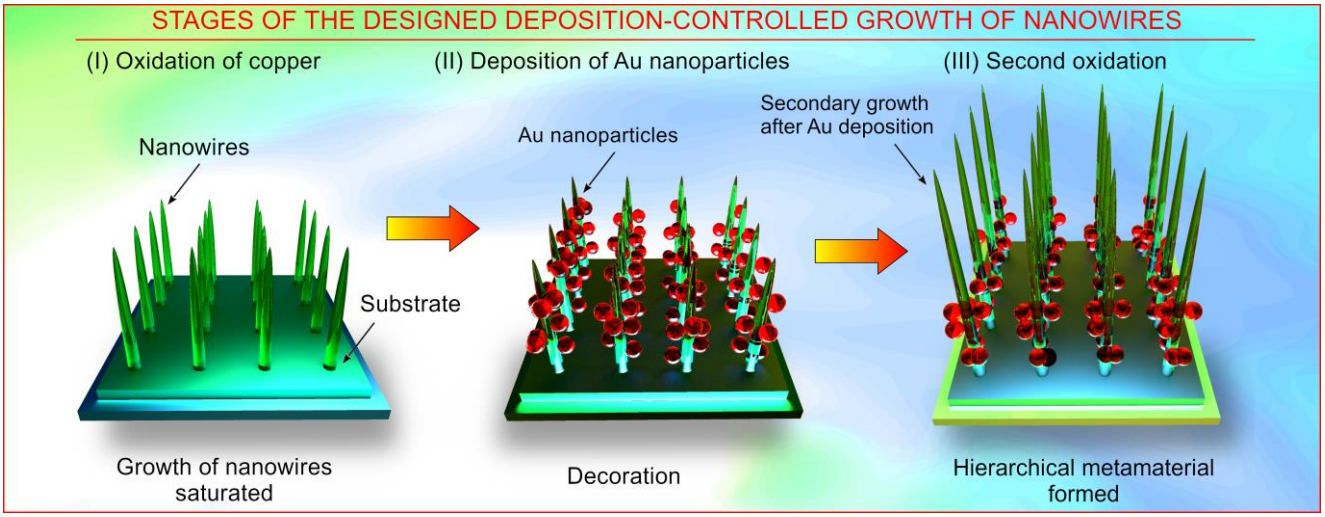

Figure 1. General scheme of the proposed process and simplified scheme of the processes during the decoration-controlled nanowire growth. Stages of the designed deposition-controlled growth of nanowires: (I) afterglow oxidation of copper; (II) deposition of Au nanoparticles; (III) second oxidation.

2. General description of the model

The fast saturation of the dependence of nanowire length on time was experimentally observed in the process that utilizes low-pressure plasma.[44] In contrast, atmospheric plasma used in this work is not associated with the ballistic effects caused by the ion bombardment, which results in less damaged surfaces of the growing nanowires. Moreover, large number of radicals ensures the high chemical activity of oxygen plasma at atmospheric pressure, as well as its ability to conduct the fast oxidation of copper substrates. At that, the substrates exhibit a formation of a layered structure of Cu_2O and CuO oxides, which are also denoted as copper (I) (or cuprous), and copper (II) (or cupric) oxides, respectively. Formation of the layers is conditioned by the interaction of oxygen molecules adsorbed on the substrate surface from the gas phase, and copper atoms diffusing towards the surface from the bulk copper. It is believed that nucleation of nanowires occurs in CuO layer, which is evidenced by a typical morphology of the nanowires protruding from this layer. Further growth of these 1D nanostructures is described by the processes of the delivery of copper atoms through the oxide layers, and diffusion of these atoms along the nanowire surface. Since oxygen is adsorbed by the side surface of the nanowires, the flux of copper atoms is decreased with the distance from the nanowire root due to the reaction of oxidation. At some time, the nanowire ceases to grow, because all copper atoms are consumed on their diffusion path to the tip. However, deposition of noble metals, like gold, protects the side surfaces from the oxygen adsorption, thus forming a shield for the copper atoms, and allowing the nanowire growth to be resumed (**Figure 2**).

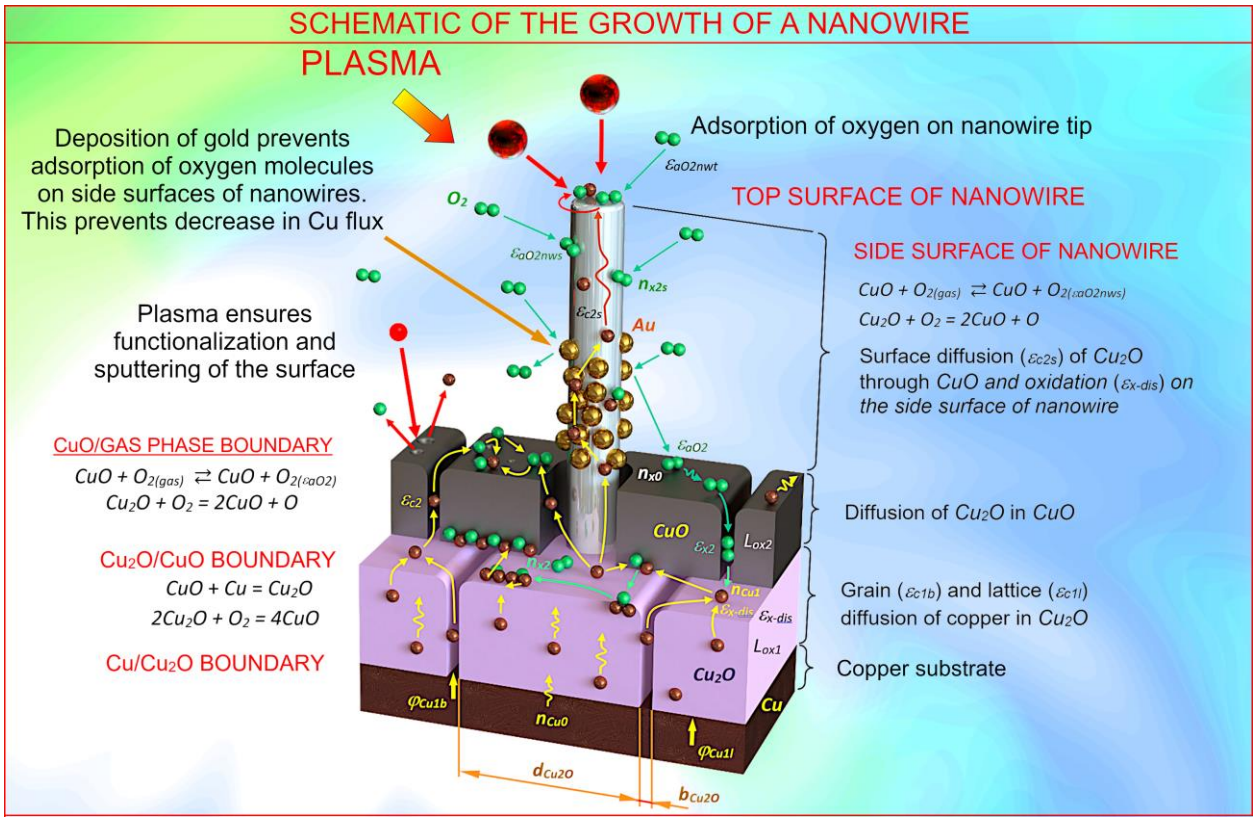

Figure 2. Schematic of the growth of nanowire partially decorated with noble metal nanoparticles. The oxide layer usually consists of two sub-layers, namely copper (II) oxide (or cupric oxide CuO), and copper (I) oxide (or cuprous oxide Cu_2O). Both oxides are formed because of the diffusion of the species, which can be lattice, boundary, or surface diffusion. In this case, the copper atoms moving from the copper layer are involved into the oxidation process on a side surface of the growing nanowire. A large number of elementary processes is involved in the growth, and all of them should be properly addressed in the advanced model (see details in the supplementary Information).

To provide a theoretical description with a purpose of establishing the possible control means when applying the stage of noble metal deposition in the process of copper oxide nanowire growth, a multifactor model was developed. The central point of the proposed strategy of intermediate deposition is to combat a growth saturation, when the nanowires stop growing at some point. Instead, after the intermediate deposition, continued growth was expected and then confirmed by simulations and direct experiment. **Figure 1** illustrates the proposed strategy (left panel) and the simplified set of the physical and chemical processes taken into account (see the full schematics of the processes in **Figure 2**). The oxide layer usually consists of two sub-layers, namely copper (II) oxide (or cupric oxide CuO), and copper (I) oxide (or cuprous oxide Cu_2O).[45,46] Both oxides are formed via lattice, boundary, and surface diffusion. The copper atoms moving from the copper layer are oxidated at the side surface of the growing nanowire, so the copper flow from the nanowire (NW) base to the NW top decreases, and the longer is the NW, the lower is the flow of copper atoms.[47] At some stage the growth is terminated because all diffusing copper is oxidized on the NW sides. The intermediate deposition of noble metal allows to resume the growth since the noble metals do not interact with the oxygen and prevents O_2 adsorption, and the surface is relatively free from the adsorbed oxygen (**Figure 3**). The copper atoms now can reach the top, copper is delivered to the NW top where it is involved into the reaction with the oxygen adsorbed on the NW top, and the NW continues to grow.

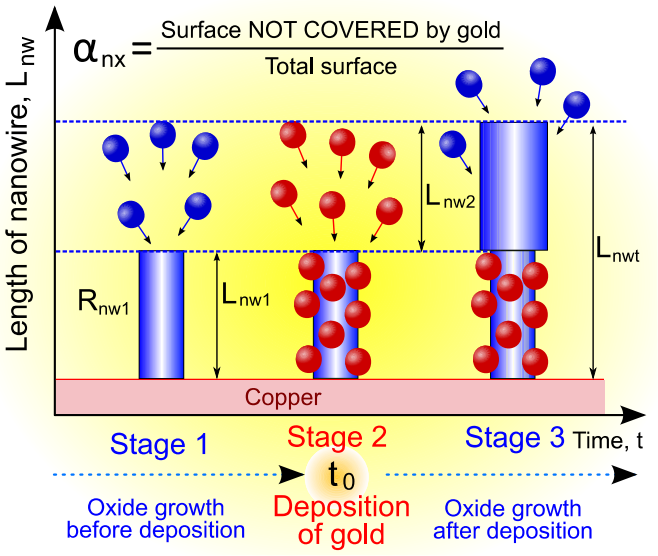

Figure 3. Scheme of controlling the nanowire array morphology by the intermediate deposition of gold. Here, t_0 is a time when gold nanoparticles are deposited on nanowire, L_{nw2} is a gold-free length of a part of the nanowire grown after gold deposition on the part L_{nw1}, L_{nwt} is a total length of the nanowire after the treatment. Intermediate deposition of noble metals (e.g. gold in the case of study) allows efficient control over the morphology of a complex nanomaterial directly during the formation process.

This mechanism was proposed, simulated with a multifactor model (see the detailed description of the model in the **Supplementary Information**, **SI**) and experimentally verified. In the model, the following scenario was used: first (see the detailed description of the model in **SI**), oxygen molecules are adsorbed on the surface of the sample and react with copper atoms which diffuse through a layer of copper oxide to the surface exposed to the oxygen. Oxygen molecules are dissociated with the two main reactions: $Cu_2O + O \rightarrow 2CuO$ and $CuO + Cu \rightarrow Cu_2O$. Importantly, the oxide boundary can be shifted because of the reactions, but *the key factor of the actual oxide layer growth is the diffusion of copper atoms from the top of the Cu_2O oxide surface to the top surface of CuO oxide*, where the generation of a new CuO oxide layer occurs (**Figure 2**).[48,49] This key process was modelled in three stages: (i) dissociation of the cuprous oxide, (ii) jump of the released copper atom into the neighbouring node occupied by the cupric oxide, and (iii) the generation of the cuprous oxide in the new location of the copper atom (see details in the **SI**).

One principal problem in modeling of such systems is the difference in the characteristic energies of the adsorbed particles on various surfaces on NW, thus all processes were modeled separately. For example, three different expressions for the Langmuir adsorption isotherm were used via three different Langmuir constants P_i:

$$P_{0i}|_{i=1,2,3} = \left(\frac{M_{O2}}{2\pi h^2}\right)^{3/2} (k_B T_s)^{5/2} exp\left[-\frac{e(\varepsilon_{ai}-\varepsilon_i)}{k_B T_s}\right], \quad (1)$$

where M_{O2} is the mass of O_2 molecule, ε_{ai} are the adsorption energies of O_2 molecule on CuO surface ($i = 1$), side surface of CuO nanowire ($i = 2$), and tip of CuO nanowire ($i = 3$), respectively; ε_i is the internal energy of O_2 molecule; h is the Planck's constant (kg×m^{2}s^{-1}); e is the elementary electric charge (C); k_B is the Boltzmann constant (kg×m^{2}s^{-2}K^{-1}); and pressure P_{0i} has the standard dimension N×m^{-2} (kg×m^{-1}s^{-2}).[50] The diffusion of copper atoms through Cu_2O layer occurs in two different ways: either through the boundaries between the oxide grains or directly through the body of the grains. On the other hand, when considering a diffusion of molecular oxygen adsorbed on the upper surface of CuO oxide to the boundary between CuO and Cu_2O, only the mechanism of the diffusion along the boundaries of CuO grains (short-circuit diffusion) was considered. The stage of the intermediate deposition results in changing the number of adsorption nodes (**Figure 2**), which could be occupied by oxygen molecules, because the deposited atoms of noble metal occupy a part of them.

The key factors of growth were calculated as follows (see the full model in the **SI** provided). In particular, the key growth parameters such as the rate of increase of the nanowire length dL_{nw}/dt and radius dR_{nw}/dt are described by the expressions:

$$\frac{dL_{nw}}{dt}(L_{nw}) = n_{Cu2Onw}(L_{nw}) cos\left[\left(\frac{n_{x2s}}{n_0}\frac{\nu_0}{D_{Cus0}} exp\left[-\frac{e(\varepsilon_{x-dis}-\varepsilon_{c2s})}{k_B T_s}\right]\right)^{1/2} L_{nw}\right] \frac{n_{x2t}}{n_0}\nu_0 exp\left(-\frac{e\varepsilon_{x-dis}}{k_B T_s}\right) a_0^3, \quad (2)$$

$$\frac{dR_{nw}}{dt}(z,t,L_{nw}) = n_{Cu2Onw}(L_{nw})\frac{n_{x2s}}{n_0}\nu_0 exp\left(-\frac{e\varepsilon_{x-dis}}{k_B T_s}\right) a_0^3 cos\left[\left(\frac{n_{x2s}}{n_0}\frac{\nu_0}{D_{Cus0}} exp\left[-\frac{e(\varepsilon_{x-dis}-\varepsilon_{c2s})}{k_B T_s}\right]\right)^{1/2} z\right], \quad (3)$$

which show strong dependence on the density of oxygen molecules adsorbed on side surface of the nanowire n_{x2s} and on the nanowire tip n_{x2t}, as well as on the current nanowire length L_{nw}. In turn, both of the parameters are exponentially dependent on the energies of adsorption ε_{aO2s} and ε_{aO2t} on the corresponding area:

$$\frac{n_{x2s}(t)}{n_0} = \alpha_{nx}\frac{P_{O2}}{\left(\frac{M_{O2}}{2\pi h^2}\right)^{3/2}(k_B T_s)^{5/2} exp\left[-\frac{e(\varepsilon_{aO2s}-\varepsilon_{i-O2})}{k_B T_s}\right]+P_{O2}}, \quad (4)$$

$$\frac{n_{x2t}(t)}{n_0} = \alpha_{nxt}\frac{P_{O2}}{\left(\frac{M_{O2}}{2\pi h^2}\right)^{3/2}(k_B T_s)^{5/2} exp\left[-\frac{e(\varepsilon_{aO2t}-\varepsilon_{i-O2})}{k_B T_s}\right]+P_{O2}}. \quad (5)$$

This fact explains the characteristic morphology of 1D objects that grow like nanowires. The difference of the adsorption energies, when $\varepsilon_{aO2s} < \varepsilon_{aO2t}$, results in much lower concentration of oxygen molecules on the side surface. It allows the atoms of copper to migrate from the nanowire root towards its tip without being involved into the reaction of oxidation on the side surface, which is accompanied by thickening of the nanowire, and to be oxidized only on the tip, where the concentration of the adsorbed oxygen is large enough. Moreover, the shape of the nanowires is affected greatly by the internal energy of oxygen molecule ε_{i-O2}, which can reverse the sign of the exponent at $\varepsilon_{aO2s} < \varepsilon_{i-O2}$, thus changing the growth conditions. The mechanism of this effect can be described by analogy of interaction of over-pressurized balloon that interacts with a surface and bursts thus releasing the internal energy stored in the balloon and transferring it to the translational energy of the motion of the balloon remnants relative to the surface. Thus, the adsorption energy of oxygen molecule is decreased when the crystalline structure of the side surface of nanowire is close to the ideal structure. Besides, the transition of energy to the internal states of the molecules additionally decreases the probability of the molecule attachment to the surface. In contrast, the defected surface of the nanowire tips is beneficial for the oxygen adsorption, oxidation of copper, and non-anisotropic growth of the nanowires. In particular, the dependence of the growth process on the adsorption energy explains why the thermally-grown nanowires possess higher aspect ratio than those obtained in plasma-

driven processes, where the nanowire surface is intensively bombarded by the plasma ions, which results in generation of defects, increase of the oxygen adsorption energy, and decrease of the aspect ratio. Moreover, as it follows from the above equations, high excitation of oxygen molecules caused by the plasma environment, can suppress the nanowire growth at all. However, there is a way to overcome the limitations caused by the oxygen adsorption by covering the side surface of the nanowires with nanoparticles of noble metals, which is described by factors α_{nx} and α_{nxt} that equal to the parts of the side surface and tip area, which are non-covered by the noble metal. The above expressions state that the concentration of the adsorbed oxygen is linearly dependent on these factors.

Much more complicated is the dependence of the concentration of copper atoms at the roots of the nanowires n_{Cu20nw} on the factors of growth including the current parameters of the system:

$$n_{Cu20nw}(L_{ox2}) = \frac{n_0}{1 + 2\frac{a_0 v_0}{2D_{0c2}} L_{ox2} \frac{n_{x2s}(t)}{n_{0s}} exp[-\varphi_{c2}] \left[\frac{2(\alpha_{c2s} exp[-\varphi_{c2s}])^{-1/2}}{R_{nw}(0)} sin[(\alpha_{c2s} exp[-\varphi_{c2s}])^{1/2} L_{nw}] + \frac{n_{x2t}}{n_{x2s}} cos[(\alpha_{c2s} exp[-\varphi_{c2s}])^{1/2} L_{nw}] \right]}$$

where $\varphi_{c2} = \frac{e(\varepsilon_{x-dis} - \varepsilon_{c2})}{k_B T_s}$, $\varphi_{c2s} = -\frac{e(\varepsilon_{x-dis} - \varepsilon_{c2s})}{k_B T_s}$, $\alpha_{c2s} = \frac{n_{x2s}}{n_0} \frac{v_0}{D_{Cus0}}$, L_{ox2} is the current thickness of CuO oxide layer. The concentration depends on the energy $\varepsilon_{x\text{-}dis}$ of oxygen molecule dissociation at the presence of Cu_2O composite, energy ε_{c2} of Cu diffusion in CuO layer, and energy ε_{c2s} of Cu diffusion along the side surface of CuO nanowire toward its tip.

The complete model comprising 50 equations was then solved numerically according to the following algorithm that enabled calculation of all essential energies, states and growth parameters (**Figure 4**). First, the initial conditions have been assigned as a typical value set for the similar experiments. Next, all essential mechanical and chemical processes were simulated. The results were presented as the growth rates described in detail in the next section.

3. Results and Discussions

A final system of the equations describing the growth was assembled (see **SI**, Equations S1 – S50) and then used for the modeling at the conditions used in the experiment. These data allowed calculating the thicknesses of both oxides, length $L_{nw}(t)$ and diameter $2R_{nw}(t)$ of nanowires on time t. **Figure 5** shows the calculated dependences of the length and diameter on growth time, moment of deposition of noble metal (gold), diffusion energy of copper along the nanowire surface ε_{c2s}, and fraction α_{nx} of the side surface of nanowires not covered with the noble metal. **Figure 5** also shows markers that correspond to the experiments by Altaweel *et al.*,[51] used as benchmarks to realistically calibrate the growth rates. At later stages the growth saturates.[52] Apparently, intermediate deposition onto the saturated nanowires allows obtaining the maximum length after secondary oxidation.

The model predicts that the maximum length is significantly affected by the energy ε_{c2s} of copper diffusion on nanowire, so we used two values of this parameter for the calculations. Importantly, the values of energies can be changed by varying concentrations of defects on the surface via ion bombardment. The lower value of the diffusion energy leads to the formation of longer nanowires – about 6.5 μm (**Figure 5b**), instead of 2.8 μm for an energy of 0.56 eV (**Figure 5a**). The dotted lines predict the growth process after gold deposition at a certain time t_i (after four, eight or twelve hours of nanowire growth). **Figures 5d,e** show the results for different values of ratio α_{nx}. When reducing α_{nxs} = 1.0 (absence of gold on the side surface of the nanowire) to α_{nxs} = 0.15 (gold covers 85% of the side surface), almost twofold increase in the length of the nanowire is predicted, i.e. the formation of long and thin nanowires is available. Importantly, the diffusion activation energy ε_{c2s} does not affect the diameter of the nanowire, while the ratio α_{nx} allows adjusting the nanowire diameter.

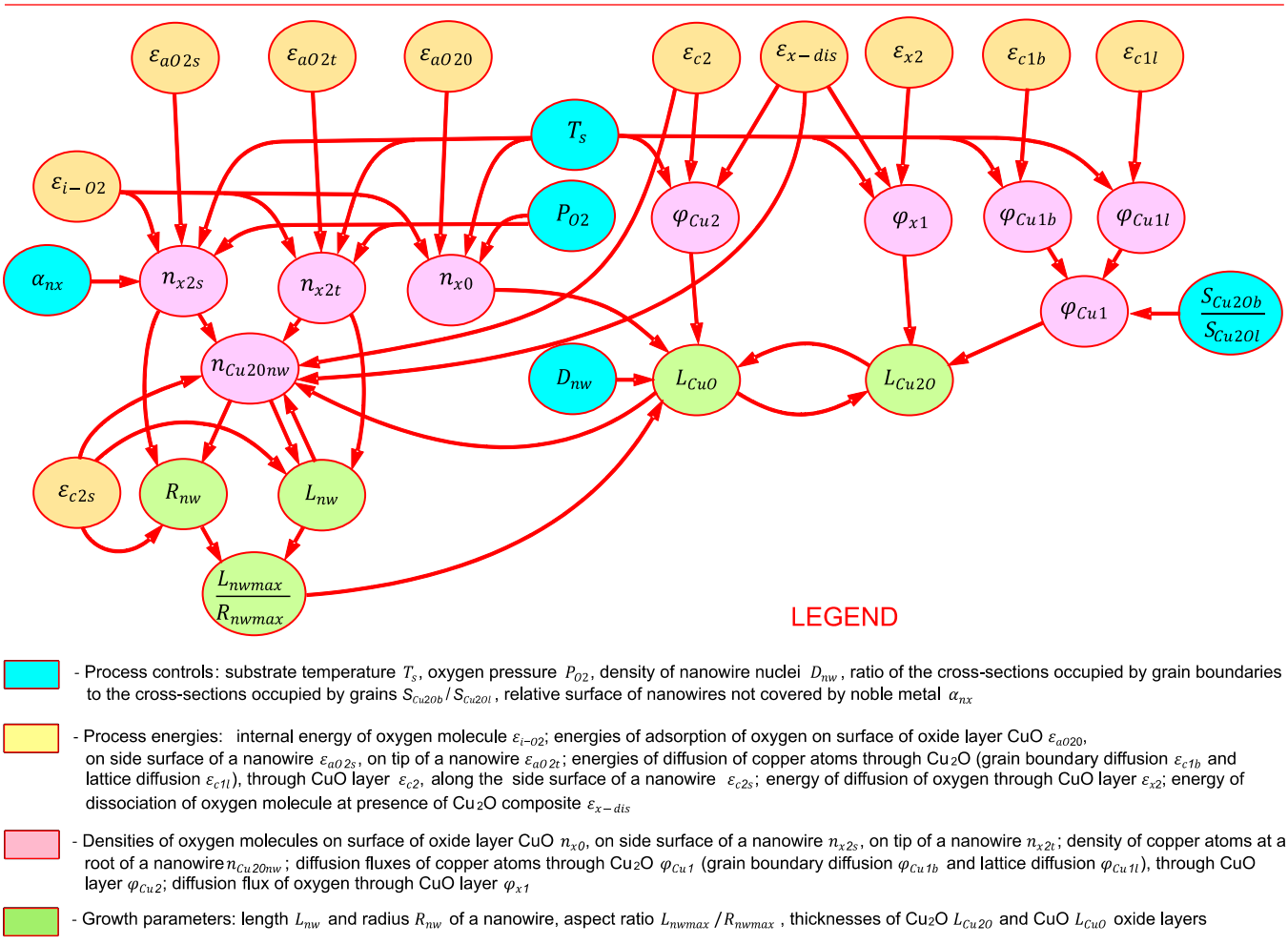

Figure 4. General scheme of the simulation for modelling the noble metal decoration-mediated growth of nanowires. Starting from setting the initial parameters typical for the experiments, the simulation route followed all essential chemical and physical processes to simulate the growth in detail (see the abbreviations for energies and other parameters in the SI provided).

Thus, under the condition of ion bombardment (ε_{c2s} = 0.56 eV) and significant coverage of the side surface with noble metal (α_{nx} = 0.15), the nanowires with a length of 9 μm and a diameter of 0.1 μm (aspect ratio 90) were produced instead of the nanowires with 3 and 0.13 μm, respectively (aspect ratio 23). When the intensity of ion bombardment is decreased (ε_{c2s} = 0.46 eV), even longer (12 μm at the maximum) nanowires with almost constant diameter along the length can be achieved. The results of 3D modelling are shown in **Figure S1**, which clearly indicates the effectiveness of the proposed approach.

Importantly, the state of the oxygen adsorbed on the nanowire surface should not be neglected, according to the simulation. The concentration of oxygen on the surface should be controlled independently by choosing the appropriate growth conditions, when the crystalline structure is not damaged by the treating fluxes, to avoid formation of large number of surface defects followed by the increase of the activation energy ε_{c2s}. It can be achieved by use of atmospheric plasma post glow, when the surface is treated by oxygen radicals and exited states, but not the oxygen ions as in the case of implementation of low-pressure plasma discharges. The 'mild' atmospheric plasma conditions are associated with lower energy ε_{c2s} and, correspondingly, longer and thinner nanowires (c, d) as compared to the case of low-pressure RF plasma, where the energy ε_{c2s} is increased due to the ion bombardment (a, b), and the nanowires becomes shorter and thicker at the saturation point.

Moreover, the radius of the upper part of the nanowire after the gold deposition exceeds the radius of the lower part (half-covered by the gold particles). This was explained by the different oxidation activity of these parts due to the gold deposit that prevents the adsorption of oxygen on the lower part, and not affects the adsorption of the side surface grown after the gold deposition. When the gold covers almost all side surface of the nanowire (α_{nxs} = 0.01), the maximal increment in the nanowire length can be obtained, as it is shown in **Figure 5e**.

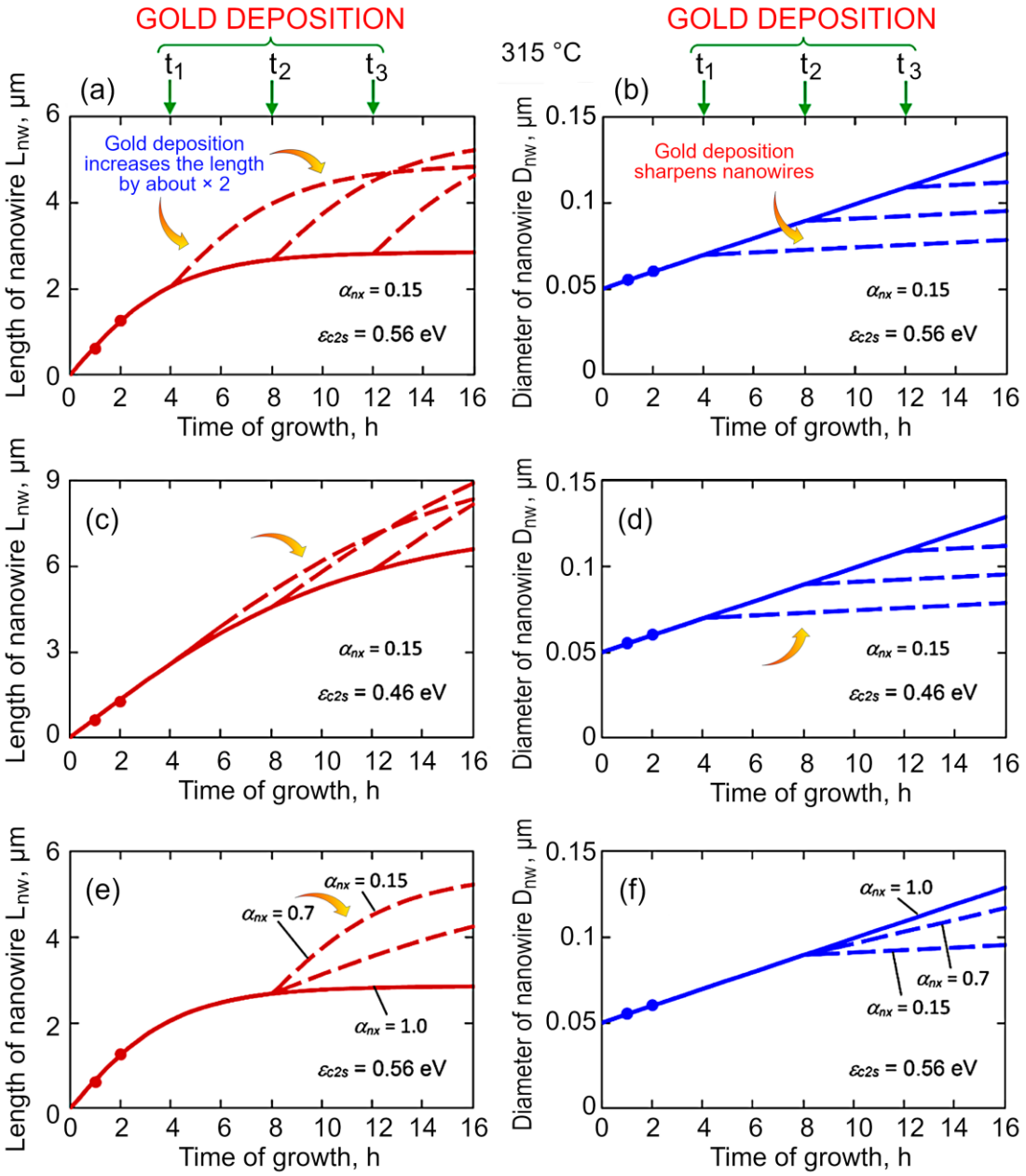

Figure 5. Results of simulations. The calculated dependences of length $L_{nw}(t)$ (a, c, e) and diameter $D_{nw}(t)$ (b, d, e) of nanowires on growth time t, moment of gold nanoparticle deposition t_i, activation energy ε_{c2s} of copper diffusion along the nanowire, and ratio α_{nxs} of the side surface not covered with gold. Solid lines describe the growth without intermediate deposition, while the golden arrows and dashed lines highlight the growth for the trends obtained for the gold-mediated growth process. Specifically, the dashed lines in (a-d) denote the growth for various moments of gold nanoparticle deposition t_i, while the dashed lines in (e,f) show the growth for different coverages (α_{nx}) of the side surface of nanowires with gold. Dots mark the experimental results.[51] Combination of the correct time moment (a, b), when the dependence of the length on time reaches the saturation, i.e., a nanowire cannot grow anymore, and a sufficient dose of deposition (when the nanoparticles of noble metal protect the already-grown surface from further oxidation, e, f) allows obtaining the best results, when two-fold increase of the nanowire length is achieved. The procedure of the gold deposition can be repeated again for the part of the nanowire grown after the previous stage of the gold deposition to lengthen the nanowire further.

To demonstrate the possible efficiency of the intermediated deposition, a faster plasma-enhanced process was used for the simulation. As was demonstrated by Filipič *et al.*,[47] when applying RF discharge to the growth of oxide structures, the dependence of a nanowire length on time reaches the saturation mode just 20 minutes after the process started. The results of the simulation using this model are also shown in **Figure 6**, where the length and diameter of the nanowires are calculated as a function of time t, moment of deposition of gold nanoparticles t_0, and ratio α_{nx}. The points shown in **Figure 6** present the experimental data reported in the cited paper. **Figure 6a** and **Figure 6b** describe the growth of a nanowire without gold deposition (α_{nx} = 1.0). The implementation of the gold deposition in the amount to cover a half of the side surface of a nanowire (α_{nx} = 0.5) changes the nanowire morphology as shown in **Figure 6c,d**. The nanowire length increased up to about 40 % (**Figure 6c**), while the change in the nanowire radius is not so significant (**Figure 6d**) as it was demonstrated in **Figure 6f**.

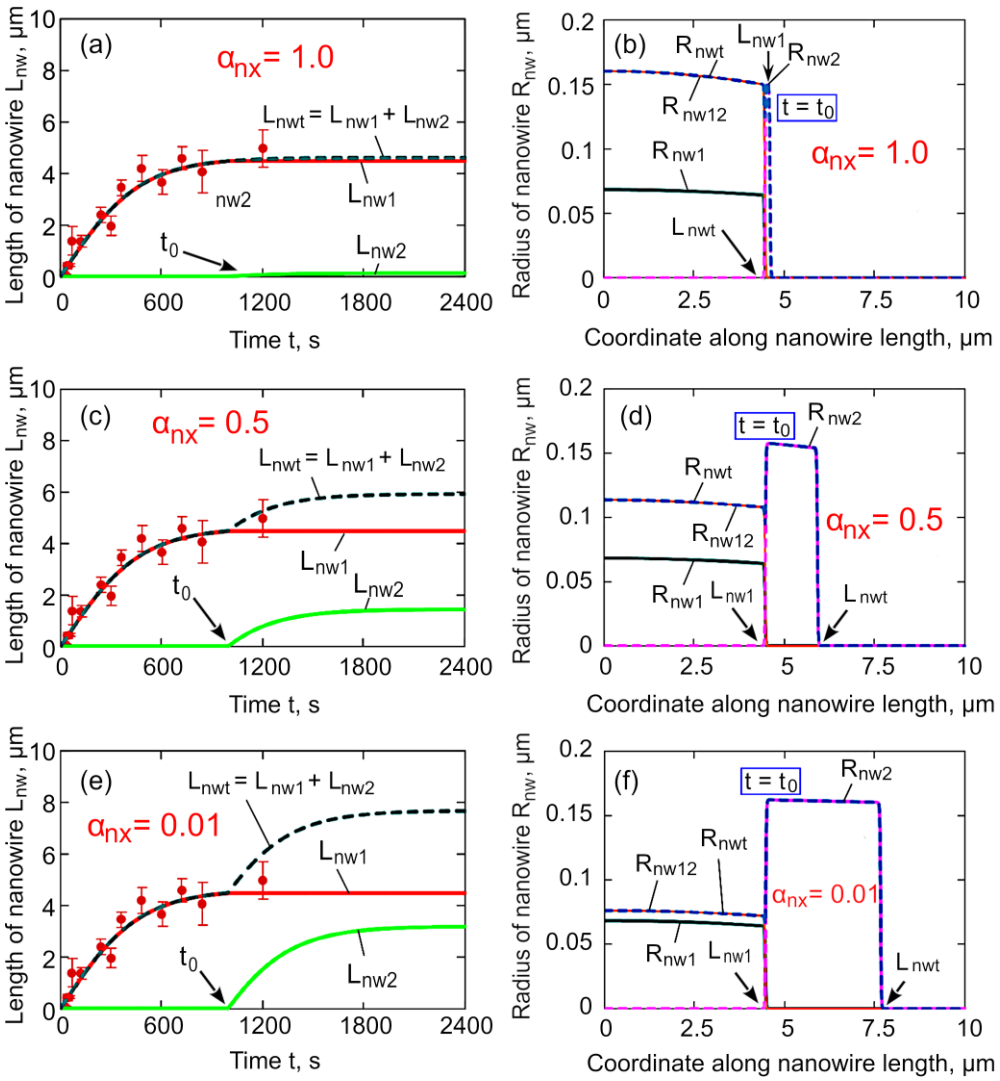

Figure 6. Results of simulations. Dependence of the nanowire length on time t (a, c, e), and shape of nanowires (b, d, f) for t = 1000 s and t = 2400 s for different coverage (α_{nx}) of side surface with gold nanoparticles. Growth of nanowire without gold deposition (α_{nx} = 1.0) (a, b); gold was deposited at t_0 = 1000 s, when the saturation mode was reached so the length of the nanowires reached its maximum, and the gold nanoparticles covered a half (c, d) of the side surface (α_{nx} = 0.5) or almost all (e, d) side surface of the nanowire (α_{nxs} = 0.01). The nanowire length and radius are L_{nw1} and R_{nw1} (b, d, f) at the moment $t = t_0$, and stay almost the same if the deposition is not conducted (b). With gold (d, f), the radius of the covered part is increased at t = 2400 s to the radius R_{nw12}, and additional substructure with a radius R_{nw2} and length L_{nw2} is formed on the tip of the nanowire, thus increasing the total length to L_{nwt} (dashed line R_{nwt} presents the final shape of the nanowires). Dots mark the experimental results.[52]

In **Figures 6a-e** the continuous red lines present the results of simulations made by use of the developed model to explain the experimental data shown by the red dots. The experiments were conducted until the saturation of the dependence of a nanowire length on time was achieved, and it was expected that further measurements will follow the red line. The black dashed lines represent the cases with deposition of gold that occurs at t_0. Thus, the red and black lines coincide up to the moment t_0. After this time moment, the dashed lines indicate the growth of the nanowires that is promoted by the deposition of gold (dotted lines). Without the deposition, the growth is terminated due to the saturation (red line after t_0). So, the deposition protects the side surface of the nanowires from the oxidation and increases the diffusion path of copper atoms, thus ensuring the increase of the nanowire length. When deposition is very small (a), the length only slightly increases and the intermediate coverage of the side surface with gold (c) results in the significant prolongation. The nanowire length is doubled when almost entire side surface is covered (e).

Figures 6a,b clearly illustrate the presence of the saturation mode in the nanowire growth observed in the experiments with low-pressure RF plasma; here a highly-defected nanowire surface formed under the condition of significant ion bombardment is suggested withing a frame of the developed model. The theoretical calculations explain the saturation by the existence of a maximal path that a flux of copper atoms, which diffuse from the nanowire root towards the tip, can overcome under a condition of the flux losses caused by the reaction of oxidation on the side surface of the nanowire. In this case, the higher concentration of adsorbed oxygen molecules on the side surface results in shortening of the diffusion path, and the ion bombardment promotes the adsorption by increasing the number of surface defects and the value of the adsorption energy. Deposition of noble metal (gold) decreases the adsorption energy thus hindering the oxygen adsorption; thus, the copper flux can overcome the longer path as is shown in **Figure 6c**. At the same time, long exposition of the nanowire that was 'armoured' by the gold nanowire at the lower part, can result in decrease of oxygen adsorption on the gold layer, or even termination (**Figure 6e**) while the tip of the nanowire that was formed after the deposition can increase its diameter with time, as it is shown in **Figure 6d**). If the gold nanoparticles cover almost the whole surface of a nanowire after the deposition stage, the mushroom-like nanostructure can be developed as is shown in **Figure 6f**.

4. Control Experiment

A direct control experiment was performed to check the simulations-derived behaviour and thus to confirm the key principles of growth control via selective noble material deposition.

A schematic of the experimental setup and the description of the process are presented in Figure S2 (SI). Microwave generator operating at 2.45 GHz and 100 W of applied power was used for growing U oxide nanowires in Ar with 10 vol.% of O_2 plasma at atmospheric pressure (see the detailed description in SI). After reaching a 600 nm length in one hour of the process, the nanowires were covered by gold nanoparticles in a metallizer and then were oxidized for one more hour. The produced materials were characterized by SEM, TEM and EDX methods (Figures S3 and S4). The lengths of the nanowires are between 1 and 1.5 μm, with a large number of nanoparticles with diameters between 2 and 5 nm observed at the base of the nanowires. On the other hand, no nanoparticle was visible at the top of the wires (Figure S3c). To confirm these observations, high resolution images were taken respectively at the top (Figure S3d) and at the base of the nanowires (Figure S3e,f). The crystal structure of the upper part of the nanowire is comparable to observations made on the nanowires without gold deposits. In particular, in the upper part of the image, the spacing between two consecutive planes is 0.25 nm, which is compatible with the lattice parameter of the (-111) plane of the monoclinic phase of CuO. To fully verify the nature of the nanoparticles, energy dispersion spectra (EDS) were acquired respectively in the middle (Figure S4a) and at the base

of the nanowires (Figure S4b). These spectra clearly show the presence of gold at the base of the nanowires. No trace of gold is visible at the top of the nanowires. In addition, a random analysis of the nanowires in the sample confirmed that the nanoparticles are only present in the lower part, approximately between the base (at the interfacial zone between the film and the wires) and the middle of the nanowire.

5. Conclusions

A method to control the nanowire growth by the intermediate deposition of nanoparticles of noble metals on a side surface of the nanowires is proposed, analysed numerically, and verified experimentally. The intermediate deposition and the nanoparticle-induced re-mapping of surface processes can drastically change the morphology of the nanowires due to the *reduction of the oxidation reactions on a side surface of the nanowires*, *shielded by noble nanoparticles*. This makes it possible for the copper atoms to diffuse along the nanowire surface from the nanowire bottom to the tip to reach *higher altitude above the level of copper oxide*, and finally *to increase to nanowire length*. According to the simulations and the verification experiment, the intermediate deposition can be a promising tool in the development of new technologies of copper oxide nanostructures.

Moreover, the experiment has presented a fundamental insight related to the longstanding question about the bottom-up and top-down growth types that vary for various materials and systems, and is quite difficult for the direct experimental verification.[53,54] In this experiment the metal nanoparticles could be considered as *markers of the nanoparticle growth zone* and they did not change their location on the nanowire during the second round of oxidation, this directly indicates that copper oxide nanowires do not grow from the bottom like human hair. This experiment provides a strong verification in favour of the assumption about the growth of copper oxide nanowires on their tips, so the nanowires increase their lengths when a new layer of material is added as a result of oxidation on the nanowire tip.

Supporting Information

Supporting Information is available free of charge from the Wile online library: (1) Description of the model, (2) Details of simulation, (3) Additional simulation results, (4) Description of the experiment, (5) Experimental results

Acknowledgements

O.B. acknowledges the support from the project funded National Research Foundation of Ukraine, under grant agreement No. 2020.02/0119 and NATO Science for Peace and Security Programme under grant id. G5814 project NOOSE. U.C. acknowledge the support from Slovenian Research Agency grant N2-0107. K.B. acknowledges funding from the Australian Research Council (FT190100819 and DP180101254) and the Australian National University Futures Scheme. I.L. acknowledges the support from the Nanyang Technological University, NIE, and the Australian National University.

Conflict of Interests

The authors declare no conflict of interest.

Keywords

Hierarchical nanomaterials, deposition, fundamental insight

References

[1] I. Levchenko, K. Bazaka, M. Keidar, S. Xu, J. Fang. Hierarchical multicomponent inorganic metamaterials: Intrinsically driven self-assembly at the nanoscale. *Adv. Mater.* **2018**, *30*, 1702226. https://doi.org/10.1002/adma.201702226

[2] C. Carra, A. Medvids, D. Litvinas, P. Ščajev, T. Malinauskas, A. Selskis, H. E. Roman, K. Bazaka, I. Levchenko, C. Riccardi. Hierarchical carbon nanocone-silica metamaterials: implications for white light photoluminescence. *ACS Appl. Nano Mater*. **2022**, *5*, 4, 4787–4800. https://doi.org/10.1021/acsanm.1c04283

[3] C.-H. Yu, B.-Y. Tseng, Z. Yang, C.-C. Tung, E. Zhao, Z.-F. Ren, S.-S. Yu, P.-Y. Chen, C.-S. Chen, M. J. Buehler. Hierarchical Multiresolution Design of Bioinspired Structural Composites Using Progressive Reinforcement Learning. *Adv. Theor. Simulations* **2022**, *5*, 2200459. https://doi.org/10.1002/adts.202200459

[4] C. Zhang, N. Wang, Y. Xu, H.-Y. Tan, Y. Feng. Identification of key contributive compounds in a herbal medicine: A novel mathematic-biological evaluation approach. *Adv. Theor. Simulations* **2021**, *4*, 2000279. https://doi.org/10.1002/adts.202000279

[5] O. Baranov, K. Bazaka, T. Belmonte, C. Riccardi, E. Roman, M. Mandhakini, S. Xu, U. Cvelbar, I. Levchenko. Recent innovations in the technology and applications of low-dimensional CuO nanostructures for sensing, energy and catalysis. *Nanoscale Horiz.* **2023,** *8*, 568-602. https://doi.org/10.1039/D2NH00546H

[6] M. A. Fadardi, T. Movlarooy. Simulation of NOx and COx gas sensor based on pristine armchair stanene nanoribbon. *Adv. Theor. Simulations* **2023**, Accepted manuscript. https://doi.org/10.1002/adts.202200875

[7] S.-J. Yang, Y.-K. Lin, Y.-C. Pu, Y.-J. Hsu. Crystal facet dependent energy band structures of polyhedral Cu_2O nanocrystals and their application in solar fuel production. *J. Phys. Chem. Lett.* **2022**, *13*, 6298-6305. https://doi.org/10.1021/acs.jpclett.2c01632

[8] C. Zhang, Z. Peng, C. Huang, B. Zhang, C. Xing, H. Chen, H. Cheng, J. Wang, S. Tang. High-energy all-in-one stretchable micro-supercapacitor arrays based on 3D laser-induced graphene foams decorated with mesoporous ZnP nanosheets for self-powered stretchable systems. *Nano Energy* **2021**, *81*, 105609. https://doi.org/10.1016/j.nanoen.2020.105609

[9] I. Levchenko, O. Baranov, C. Riccardi, H. E. Roman, U. Cvelbar, E. P. Ivanova, M. Mohandas, P. Ščajev, T. Malinauskas, S. Xu, K. Bazaka. Nanoengineered carbon-based interfaces for advanced energy and photonics applications: A recent progress and innovations. *Adv. Mater. Interfaces* **2023**, *10*, 2201739. https://doi.org/10.1002/admi.202201739

[10] Z. Chen, S. Zhang, I. Levchenko, I. I. Beilis, M. Keidar. In vitro demonstration of cancer inhibiting properties from stratified self-organized plasma-liquid interface. *Sci. Rep.* **2017**, *7*, 12163. https://doi.org/10.1038/s41598-017-12454-9

[11] P. Liu, G. Wang, Q. Ruan, K. Tang, P. K. Chu, Plasma-activated interfaces for biomedical engineering, *Bioactiv*. *Mater*. **2021**, *6*, 2134-2143. https://doi.org/10.1016/j.bioactmat.2021.01.001

[12] K. Li, Y. de Rancourt de Mimérand, X. Jin, J. Yi, J. Guo, Metal Oxide [ZnO and TiO_2] and Fe-Based metal–organic-framework nanoparticles on 3D-printed fractal polymer surfaces for photocatalytic degradation of organic pollutants, *ACS Appl. Nano Mater*. **2020**, *3*, 2830-2845. https://doi.org/10.1021/acsanm.0c00096

[13] Q. Xiang, X. Ma, D. Zhang, H. Zhou, Y. Liao, H. Zhang, S. Xu, I. Levchenko, K. Bazaka. Interfacial modification of titanium dioxide to enhance photocatalytic efficiency towards H_2 production. *J. Colloid Interface Sci*. **2019**, *556*, 376-385. https://doi.org/10.1016/j.jcis.2019.08.033

[14] R. Réocreux, E. C. H. Sykes, A. Michaelides, M. Stamatakis. Stick or spill? Scaling relationships for the binding energies of adsorbates on single-atom alloy catalysts. *J. Phys. Chem. Lett.* **2022**, *13*, 7314-7319. https://doi.org/10.1021/acs.jpclett.2c01519

[15] S. Sasi, K. Prasad, J. Weerasinghe, O. Bazaka, E. P. Ivanova, I. Levchenko, K. Bazaka. Plasma for aquaponics. *Trends Biotechnol.* **2023**, *41*, 46-62. https://doi.org/10.1016/j.tibtech.2022.08.001

[16] A. Kumar, A. Aljumaili, O. Bazaka, E. P. Ivanova, I. Levchenko, K. Bazaka, M. Functional nanomaterials, synergism and biomimicry for environmentally benign marine antifouling technology. *Mater. Horiz.* **2021**, *8*, 3201-3238. https://doi.org/10.1039/D1MH01103K

[17] Y. Xu, M. Fan, W. Yang, Y. Xiao, L. Zeng, X. Wu, Q. Xu, C. Su, Q. He. Homogeneous carbon/potassium-incorporation strategy for synthesizing red polymeric carbon nitride capable of near-infrared photocatalytic H_2 production. *Adv. Mater.* **2021**, *33*, 2101455. https://doi.org/10.1002/adma.202101455

[18] X. Zhang, Y. Liu, Nanomaterials for radioactive wastewater decontamination, *Environ. Sci.: Nano* **2020**, *7*, 1008-1040. http://dx.doi.org/10.1039/C9EN01341E

[19] I. Levchenko, K. Bazaka, T. Belmonte, M. Keidar, S. Xu. Advanced materials for next generation spacecraft. *Adv. Mater*. **2018,** *30*, 1802201. https://doi.org/10.1002/adma.201802201

[20] I. Levchenko, M. Keidar, J. Cantrell, Y.-L. Wu, H. Kuninaka, K. Bazaka, S. Xu. Explore space using swarms of tiny satellites. *Nature* **2018**, *562*, 185-187. https://doi.org/10.1038/d41586-018-06957-2

[21] N. Singhal, I. Levchenko, S. Huang, L. Xu, G.-C. Potrivitu, O. Cherkun, J. Fang, K. Bazaka, S. Xu. 3D-Printed multilayered reinforced material system for gas supply in cubeSats and small satellites. *Adv. Eng. Mater.* **2019**, *21*, 1900401. https://doi.org/10.1002/adem.201900401

[22] I. Levchenko, S. Xu, G. Teel, D. Mariotti, M. L. R. Walker, M. Keidar. Recent progress and perspectives of space electric propulsion systems based on smart nanomaterials. *Nat. Commun*. **2018,** *9*, 879. https://doi.org/10.1038/s41467-017-02269-7

[23] B. Guo, M. Košiček, J. Fu, Y. Qu, G. Lin, O. Baranov, J. Zavašnik, Q. Cheng, K. Ostrikov and U. Cvelbar, Single-crystalline metal oxide nanostructures synthesized by plasma-enhanced thermal oxidation, *Nanomaterials* **2019**, *9*, 1405. https://doi.org/10.3390/nano9101405

[24] Y. Su, T. Liu, P. Zhang, P. Zheng, CuO nanowire arrays synthesized at room temperature as a high-performance anode material for Li/Na-ion batteries, *Thin Solid Films* **2019**, *690*, 137522. https://doi.org/10.1016/j.tsf.2019.137522

[25] C. Tang, X. Liao, W. Zhong, H. Yu, Z. Liu, Electric field assisted growth and field emission properties of thermally oxidized CuO nanowires, *RSC Adv*. **2017**, *7*, 6439–6446. https://doi.org/10.1039/c6ra27426a

[26] C. S. Lee, J. Bae, Room-temperature growth ["farming"] and high-performance supercapacitor applications of highly crystalline CuO nanowires/graphene nanoplatelet nanopowders, *J. Mater. Sci. – Mater. El.* **2018**, *29*, 15097–15105. https://doi.org/10.1007/s10854-018-9650-7

[27] D. Majumdar, S. Ghosh, Recent advancements of copper oxide-based nanomaterials for supercapacitor applications, *J. Energy Storage* **2021**, *34*, 101995, https://doi.org/10.1016/j.est.2020.101995

[28] S. Steinhauer, Gas Sensors Based on Copper Oxide Nanomaterials: A Review, *Chemosensors* **2021**, *9*, 51, https://doi.org/10.3390/chemosensors9030051

[29] V. H. Luan, J. H. Han, H. W. Kang, W. Lee, Highly porous and capacitive copper oxide nanowire/graphene hybrid carbon nanostructure for high-performance supercapacitor electrodes, *Composites Part B* **2019**, *178*, 107464, https://doi.org/10.1016/j.compositesb.2019.107464

[30] T. Ma, L. Gao, Y. Liu, L. Zhang, X. Yang, Porous CuO/Cu2O heterostructured arrays as anode for high-performance sodium-ion batteries, *Ionics* **2021**, *27*, 1995-2003, https://doi.org/10.1007/s11581-021-03968-4

[31] A. Ghosh, M. Miah, A. Bera, S. K. Saha, B. Ghosh, Synthesis of freestanding 2D CuO nanosheets at room temperature through a simple surfactant free co-precipitation process and its application as electrode material in supercapacitors, *J. Alloys Compounds* **2021**, *862*, 158549, https://doi.org/10.1016/j.jallcom.2020.158549

[32] A. Shariffar, H. Salman, T. A. Siddique, M. O. Manasreh, Effects of high-temperature annealing on the performance of copper oxide photodetectors, *Appl. Phys. A* **2021**, *127*, 750. https://doi.org/10.1007/s00339-021-04906-x

[33] R. Kottappara, S. Palantavida, S. C. Pillai, B. K. Vijayan, Hollow 1D copper oxide nanostructures with enhanced activity for catalytic reduction and photocatalytic degradation of organic pollutants, *Surfaces and Interfaces* **2021**, *22*, 100876, https://doi.org/10.1016/j.surfin.2020.100876

[34] S. Kulkarni, R. Ghosh, A simple approach for sensing and accurate prediction of multiple organic vapors by sensors based on CuO nanowires, *Sensors & Actuators: B. Chemical* **2021**, *335*, 129701, https://doi.org/10.1016/j.snb.2021.129701

[35] D. Gizinski, A. Brudzisz, M. R. Alzahrani, K.-K. Wang, W. Z. Misiołek, W. J. Stepniowski, Formation of CuOx Nanowires by Anodizing in Sodium Bicarbonate Solution, *Crystals* **2021**, *11*, 624, https://doi.org/10.3390/cryst11060624

[36] S. H. Mohamed, K. M. Al-Mokhtar, Characterization of Cu_2O/CuO nanowire arrays synthesized by thermal method at various temperatures, *Appl. Phys. A*, **2018**, *124*, 493. https://doi.org/10.1007/s00339-018-1914-9

[37] I. Levchenko, M. Mandhakini, K. Prasad, O. Bazaka, E. P. Ivanova, M. V. Jacob, O. Baranov, C. Riccardi, H. E. Roman, S. Xu, K. Bazaka. Functional nanomaterials from waste and low-value natural products: A technological approach level. Adv. Mater. Technol. **2022**, *7*, 2101471. https://doi.org/10.1002/admt.202101471

[38] L. Feng, H. Yan, H. Li, R. Zhang, Z. Li, R. Chi, S. Yang, Y. Ma, B. Fu, J. Liu, Excellent field emission properties of vertically oriented CuO nanowire films, *AIP Adv.* **2018**, *8*, 045109. https://doi.org/10.1063/1.5022320

[39] L. Nkhaili, A. Narjis, A. Agdad, A. Tchenka, A. El Kissani, A. Outzourhit, A. Oueriagli, A simple method to control the growth of copper oxide nanowires for solar cells and catalytic applications, *Adv. Cond. Matter. Phys.* **2020,** *2020*, 1–8. https://doi.org/10.1155/2020/5470817

[40] F. Cao, S. Jia, H. Zheng, L. Zhao, H. Liu, L. Li, L. Zhao, Y. Hu, H. Gu, J. Wang, Thermal-induced formation of domain structures in CuO nanomaterials, *Phys. Rev. Mater*. **2017**, *1*, 053401. https://doi.org/10.1103/PhysRevMaterials.1.053401

[41] R. Sondors, J. Kosmaca, G. Kunakova, L. Jasulaneca, M. M. Ramma, R. Meija, E. Kauranens, M. Antsov, D. Erts, Size distribution, mechanical and electrical properties of CuO nanowires grown by modified thermal oxidation methods, *Nanomaterials* **2020**, *10*, 1051. https://doi.org/10.3390/nano10061051

[42] G. Fritz-Popovski, F. Sosada-ludwikowska, A. Köck, J. Keckes, G.A. Maier, Study of CuO Nanowire Growth on Different Copper Surfaces, *Sci. Rep.* **2019**, *9*, 1–13. https://doi.org/10.1038/s41598-018-37172-8

[43] I. Levchenko, S. Xu, O. Baranov, O. Bazaka, E. P. Ivanova, K. Bazaka. Plasma and polymers: Recent progress and trends. *Molecules* **2021**, *26*, 4091. https://doi.org/10.3390/molecules26134091

[44] O. Baranov, G. Filipič, U. Cvelbar, Towards a highly-controllable synthesis of copper oxide nanowires in radio-frequency reactive plasma: fast saturation at the targeted size. *Plasma Sources Sci. Technol*. **2019**, *28*, 084002. https://doi.org/10.1088/1361-6595/aae12e

[45] O. Baranov, G. Filipič, U. Cvelbar, Towards a highly-controllable synthesis of copper oxide nanowires in radio-frequency reactive plasma: fast saturation at the targeted size, *Plasma Sources Science and Technology* **2019**, *28*, 084002 https://doi.org/10.1088/1361-6595/aae12e

[46] O. Baranov, M. Košiček, G. Filipič, U. Cvelbar, A deterministic approach to the thermal synthesis and growth of 1D metal oxide nanostructures, *Appl. Surf. Sci.* **2021**, *566*, 150619. https://doi.org/10.1016/j.apsusc.2021.150619

[47] G. Filipič, O. Baranov, M. Mozetic, K. Ostrikov, U. Cvelbar, Uniform surface growth of copper oxide nanowires in radiofrequency plasma discharge and limiting factors, *Phys. Plasmas* **2014**, *21*, 113506, https://doi.org/10.1063/1.4901813

[48] A. Brady-Boyd, E. Chery, S. Armini. Investigating the efficacy of hafnium dioxide barrier layers to halt copper oxide formation in redistribution layers for three-dimensional [3D] packaging. *J. Phys. Chem. Lett*. **2022**, *13*, 8130–8133. https://doi.org/10.1021/acs.jpclett.2c02080

[49] L. N. Walters, E. L. Wang, J. M. Rondinelli. Thermodynamic descriptors to predict oxide formation in aqueous solutions. *J. Phys. Chem*. *Lett*. **2022**, *13*, 6236-6243. https://doi.org/10.1021/acs.jpclett.2c01173

[50] C. Kittel, and H. Kroemer, Thermal Physics, W. H. Freeman and Co, New York, **1980**.

[51] A. Altaweel, G. Filipič, T. Gries, T. Belmonte, Controlled growth of copper oxide nanostructures by atmospheric pressure micro-afterglow, *J. Crystal Growth* **2014**, *407*, 17-24. https://doi.org/10.1016/j.jcrysgro.2014.08.029

[52] G. Filipič, O. Baranov, M. Mozetic, U. Cvelbar, Growth dynamics of copper oxide nanowires in plasma at low pressures, *J. Appl. Phys.* **2015**, *117*, 043304, https://doi.org/10.1063/1.4906501

[53] B. P. Isaacoff K. A. Brown. Progress in Top-Down Control of Bottom-Up Assembly. *Nano Lett.* **2017**, *17*, 6508–6510. https://doi.org/10.1021/acs.nanolett.7b04479

[54] H. Sun, F. Liu, L. Zhang, K. Ko, B. McLean, H. An, S. Kim, M. Huang, M.-G. Willinger, R. S. Ruoff, J. Suh, Z.-J.Wang, F. Ding. Bottom-Up Growth of Graphene Nanospears and Nanoribbons. *Adv. Func. Mater.* **2022**, *32*, 2206961. https://doi.org/10.1002/adfm.202206961

Supporting Information

Hierarchical nanomaterials by selective deposition of noble metal nanoparticles: Insight into control and growth processes

Oleg Baranov[1,2], Thierry Belmonte[3], Igor Levchenko[4,5], Kateryna Bazaka[4], Martin Košiček[1,6] and Uroš Cvelbar[1,6*]*

[1] *Jožef Stefan International Postgraduate School, Ljubljana, Slovenia (EU)*
[2] *Plasma Laboratory, National Aerospace University, Kharkiv, Ukraine*
[3] *Université de Lorraine, CNRS, IJL, F-54000 Nancy, France (EU)*
[4] *School of Engineering, The Australian National University, ACT 2601, Australia*
[5] *Plasma Sources and Application Center, NIE, Nanyang Technological University, Singapore 639798*
[6] *Jožef Stefan Institute, Ljubljana, Slovenia (EU)*

*Corresponding author email: O.Baranov@khai.edu and uros.cvelbar@ijs.si

Table of Contents

1. Description of the model
2. Details of simulation
3. Additional simulation results
4. Description of the experiment
5. Experimental results

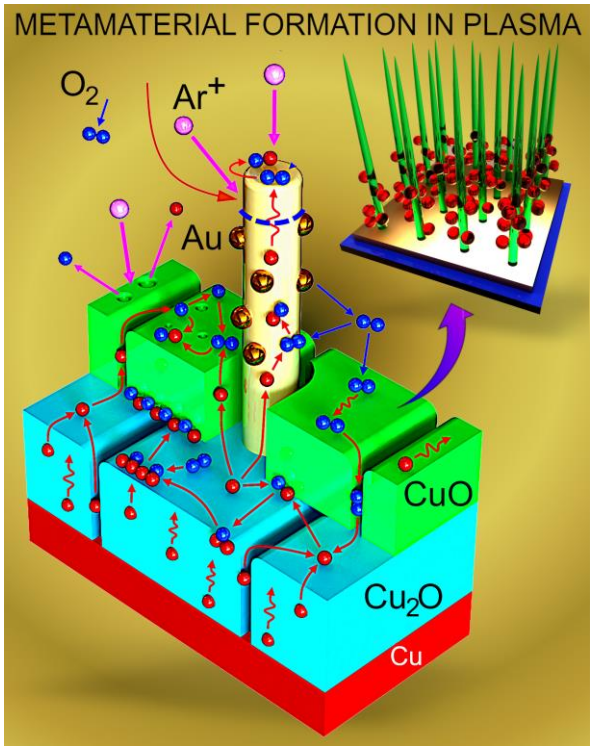

1. Description of the model

To provide a theoretical description with a purpose of establishing the possible control means when applying the stage of noble metal deposition in the process of copper oxide nanowire growth, a multifactor model was developed. A schematic of the nanowire growth at presence of noble metal of the side surface of a nanowire is shown in **Figure 2**.

In the model, the following reactions on a copper sample and oxide layers that are formed on the sample as a result of its oxidation after exposure to oxygen environment are discussed. First of all, oxygen molecules adsorb on the surface of the sample where they meet copper atoms that diffuse from a layer of copper through a layer of copper oxide to the surface of the oxide exposed to the oxygen atmosphere.

Oxygen molecules are dissociated at the oxidation of Cu_2O. The released oxygen and by-diffusion-delivered copper atoms are subject to the following reactions:

$$Cu_2O + O \rightarrow 2CuO, \tag{S1}$$

$$CuO + Cu \rightarrow Cu_2O. \tag{S2}$$

The oxide boundary can be shifted because of the reactions, but the key factor of the actual oxide layer growth is the diffusion of copper atoms from the top of the Cu_2O oxide surface to the top surface of CuO oxide, where the generation of a new CuO oxide layer occurs.

To describe the copper diffusion to the surface of the oxide we considered a three-stage process: dissociation of the cuprous oxide, "jump" of the released copper atom into the neighbouring node occupied by the cupric oxide, and the generation of the cuprous oxide in the new location of the copper atom; the following reactions take place:

$$Cu_2O \rightarrow CuO + Cu \rightarrow Cu_2O \tag{S3}$$

This last process can be considered as diffusion of Cu_2O oxide into CuO oxide: the copper atom reacts with the CuO oxide at each "jump" in that case. When the generated Cu_2O composition reaches the upper layer of the CuO oxide, it can be involved into reaction (S1) where the new CuO adsorption node is generated, which results in growing of the CuO oxide layer.

The adsorption of oxygen molecules can occur on a surface of oxide (CuO) layer (n_{x0}, m^{-2}), on a side surface of a nanowire (n_{x2s}, m^{-2}), as well as on a tip (n_{x2t}, m^{-2}) of the nanowires. The densities are related to a density of the adsorption nodes, which is a surface density of atoms of CuO oxide n_0. Due to the difference in the energies of the adsorption, three different expressions of the same form of Langmuir adsorption isotherm are used [1]:

$$\begin{aligned} \frac{n_{x0}}{n_0} &= \frac{P_{O2}}{P_{00}+P_{O2}}, \\ \frac{n_{x2s}}{n_0} &= \frac{P_{O2}}{P_{0s}+P_{O2}}, \\ \frac{n_{x2t}}{n_0} &= \frac{P_{O2}}{P_{0t}+P_{O2}}. \end{aligned} \tag{S4}$$

where P_{00}, P_{0s}, P_{ot} are the constants that depend on surface temperature, and P_{O2} is the partial pressure of oxygen, Pa; the constants are expressed as

$$P_{0i} = \left(\frac{M_{O2}}{2\pi h^2}\right)^{3/2} (k_B T_s)^{5/2} exp\left[-\frac{e(\varepsilon_{aO2i}-\varepsilon_{i-O2})}{k_B T_s}\right], \tag{S5}$$

where M_{O2} is the mass of O_2 molecule, kg; ε_{aO2i} are the adsorption energies (eV) of O_2 molecule on CuO surface ($i \rightarrow 0$), side surface of CuO nanowire ($i \rightarrow s$), and tip of CuO nanowire ($i \rightarrow t$), respectively; $\varepsilon_{i\text{-}O2}$ is the internal energy (eV) of O_2 molecule.

According to the literature [2], copper atoms can diffuse through Cu_2O layer in two different ways: either through the boundaries between the oxide grains (this flux is designated as φ_{Cu1b}) or directly through the body of the grains (this flux is designated as φ_{Cu1l}). The total flux of the copper atoms diffusing from the copper part of the sample to the boundary between Cu_2O and CuO oxides considers the relative cross-sections occupied by the inter-grain boundaries or grains:

$$\varphi_{Cu1} = P_{Cu1b}\varphi_{Cu1b} + P_{Cu1l}\varphi_{Cu1l}, \tag{S6}$$

where P_{Cu1b} and P_{Cu1l} are the ratio of the cross-sections associated with two mechanisms, respectively, to the total cross-section:

$$P_{Cu1b} = \frac{S_{Cu2Ob}}{S_{Cu2Ob}+S_{Cu2Ol}}, \qquad P_{Cu1l} = \frac{S_{Cu2Ol}}{S_{Cu2Ob}+S_{Cu2Ol}}. \tag{S7}$$

where S_{Cu2Ob} and S_{Cu2Ol} are the cross-sections occupied by the grain boundaries and grains, respectively.

In turn, they are expressed as:

$$S_{Cu2Ob} = \frac{\pi\left(d_{Cu2O}+\frac{b_{Cu2O}}{2}\right)^2}{4} - \frac{\pi d_{Cu2O}^2}{4} = \frac{\pi d_{Cu2O}^2}{4}\left(\left(1+\frac{b_{Cu2O}}{2d_{Cu2O}}\right)^2 - 1\right), \qquad S_{Cu2Ol} = \frac{\pi d_{Cu2O}^2}{4}, \tag{S8}$$

where d_{Cu2O} and b_{Cu2O} are a diameter of Cu_2O grain a thickness of the grain boundary, respectively.

After substitution, one may obtain:

$$P_{Cu1b} = \left(\left[1+\frac{b_{Cu2O}}{2d_{Cu2O}}\right]^2 - 1\right)\left(1+\frac{b_{Cu2O}}{2d_{Cu2O}}\right)^{-2}, \qquad P_{Cu1l} = \left(1+\frac{b_{Cu2O}}{2d_{Cu2O}}\right)^{-2}. \tag{S9}$$

It is assumed that copper atoms delivered to the boundary between the oxides, are consumed at their interaction with CuO layer according to reaction (2), and this reaction is a driving force of the diffusion; any reactions in the volume of Cu_2O layer of a thickness L_{ox1} are not considered. Then a density $n_{cu}(z)$ of the copper atoms is:

$$D_{Cu1i}\frac{d^2 n_{Cui}}{dz^2} = 0, \tag{S10}$$

$$n_{Cu} - n_{Cu0} = -\frac{\varphi_{Cu1i}}{D_{Cu1i}}a_0 L_{ox1}, \tag{S11}$$

where D_{Cu1i} is a diffusion coefficient, which is dependent on the temperature T_s, potential well ε_{c1i}, numerical coefficient α_{Dc1}, and lattice vibration frequency ν_0:

$$D_{Cu1i} = D_{0c1i}exp\left[-\frac{e\varepsilon_{c1i}}{k_B T_s}\right] = \alpha_{Dc1i}\frac{\nu_0 a_0^2}{2}exp\left[-\frac{e\varepsilon_{c1i}}{k_B T_s}\right], \tag{S12}$$

In turn, the latter depends on the temperature [3]:

$$\nu_0 = \frac{2k_B T_s}{h}, \tag{S13}$$

where h is the Plank's constant.

To describe the fluxes through the boundaries between Cu_2O grains and the volume of Cu_2O grain, indexes "b" or "l" should be substituted.

The fluxes delivered to the boundary between the oxides ($z = L_1$), are

$$\varphi_{Cu1i} = \frac{1}{2}n_{Cu}\nu_0 exp\left[-\frac{e\varepsilon_{c1i}}{k_B T_s}\right]. \tag{S14}$$

A dependence of the fluxes on thickness of Cu2O layer can be found by combining the equations (S11) and (S14):

$$\varphi_{Cu1i} = \frac{1}{1+\frac{a_0\nu_0}{2D_{0c1i}}L_{ox1}}\frac{n_{Cu0}\nu_0}{2}exp\left[-\frac{e\varepsilon_{c1i}}{k_B T_s}\right]. \tag{15}$$

Then, the total flux of copper atoms supplied to the CuO/Cu_2O boundary can be found:

$$\varphi_{Cu1} = \left(\frac{1}{\left(1+\frac{d_{Cu20}}{2b_{Cu20}}\right)\left(1+\frac{a_0\nu_0}{2D_{0c1b}}L_{ox1}\right)} exp\left[-\frac{e\varepsilon_{c1b}}{k_B T_s}\right] + \frac{1}{\left(1+\frac{2b_{Cu20}}{d_{Cu20}}\right)\left(1+\frac{a_0\nu_0}{2D_{0c1l}}L_{ox1}\right)} exp\left[-\frac{e\varepsilon_{c1l}}{k_B T_s}\right] \right) \frac{n_{Cu0}\nu_0}{2}, \quad \text{(S16)}$$

where a_0 is Cu_2O lattice parameter; n_{cu0} is the surface density of atoms of the copper sample, m^{-2}.

When considering a diffusion of molecular oxygen adsorbed on the upper surface of CuO oxide to the boundary between CuO and Cu_2O, only the mechanism of the diffusion along the boundaries of CuO grains (short-circuit diffusion) is taken into account. When the molecule reaches the boundary between the oxides, thermal dissociation of O_2 at presence of Cu_2O oxide occurs. At that, the flux of oxygen molecules does not react on the way to the inter-oxide boundary. Thus, the flow φ_{x2} of the oxygen molecules can be found similarly to the flows of copper atoms through Cu_2O layer:

$$n_{x2} - n_{x0} = -\frac{\varphi_{x2} a_0}{D_{0x2}} L_{ox2}, \quad \text{(S17)}$$

where D_{0x2} is a constant; n_{x0} is the surface density of adsorbed oxygen molecules on the top surface of CuO oxide, m^{-2}; L_{ox2} is a current length of CuO layer.

Under a condition that one molecule of oxygen can decay to two atoms when contacting with Cu_2O, the flux of oxygen atoms to the boundary between the oxide is:

$$\varphi_{x1} = n_{x1}\nu_{x-dec} = 2n_{x2}\nu_{x-dec} = 2n_{x2}\frac{\nu_0}{2} exp\left(-\frac{e\varepsilon_{x2}}{k_B T_s}\right) exp\left(-\frac{e\varepsilon_{x-dis}}{k_B T_s}\right) = n_{x2}\nu_0 exp\left(-\frac{e(\varepsilon_{x2}+\varepsilon_{x-dis})}{k_B T_s}\right), \quad \text{(S18)}$$

where ε_{x2} is a potential well for physisorption on the CuO grain, eV; n_{x2} is a surface density of the oxygen molecules at the boundary between the CuO and Cu_2O oxides, while n_{x1} is a surface density of oxygen atoms after the dissociation; $\nu_0/2\, exp(-e(\varepsilon_{x2} + \varepsilon_{x-dis})/k_B T_s)$ is a frequency of the jumps of O_2 toward Cu_2O oxide from CuO oxide and dissociation at the jump, $\varepsilon_{x\text{-}dis}$ is the energy of the dissociation at the presence of Cu_2O.

By combining equations (S17) and (S18), the flux of oxygen atoms to the boundary between CuO and Cu_2O is:

$$\varphi_{x1} = \frac{n_{x0}}{1+\frac{a_0\nu_0}{2D_{0x2}}L_{ox2}} \frac{\nu_0}{2} exp\left(-\frac{e(\varepsilon_{x2}+\varepsilon_{x-dis})}{k_B T_s}\right). \quad \text{(S19)}$$

A counter flux of copper atoms from the Cu_2O/CuO boundary to the top of the CuO oxide is found by use of the speculations like the above:

$$\varphi_{Cu2} = \frac{1}{2} n_{Cu2} \frac{n_{x0}}{n_0} \nu_{c2} = \frac{n_{x0}}{1+\frac{a_0\nu_0}{2D_{0c2}}L_{ox2}} \frac{\nu_0}{2} exp\left(-\frac{e(\varepsilon_{c2}+\varepsilon_{x-dis})}{k_B T_s}\right), \quad \text{(S20)}$$

where D_{0c2} is a constant; n_{Cu2} is a surface density of the copper atoms present in the form of Cu_2O oxide at the top of CuO oxide; n_{x0}/n_0 is a probability to find an adsorbed oxygen molecule on the surface of the CuO oxide; ν_{c2} is a frequency of the jumps of the copper atom toward O_2 molecule from Cu_2O oxide and dissociation of the oxide at the jump, ε_{c2} is the energy of dissociation at the reaction (S3).

Unlike the growth of CuO and Cu_2O layers, the diffusion of copper from the bottom part of a nanowire to its tip is accompanied with loss of copper flux due to reaction of oxidation (S1) oxidation on the side surface and top of the nanowire. However, by considering the fact that the nanowire roots are submerged into the layer of CuO oxide, a part of the flux of copper is not oxidised while diffusing along the nanowire root. At that the density n_{Cu20nw} of copper atoms at the bottom of a nanowire is connected with the initial density n_{Cu20} of copper atoms by the equation:

$$n_{Cu20nw} = n_{Cu20} - \frac{\varphi_{Cu2nw}}{D_{Cu2}} a_0 L_{ox2} = n_0 - \frac{\varphi_{Cu2nw}}{D_{0c2} exp\left(-\frac{e\varepsilon_{c2}}{k_B T_s}\right)} a_0 L_{ox2}. \quad \text{(S21)}$$

where the density n_{Cu20} is considered to be equal to n_0, since this is the density of Cu_2O in the Cu_2O/CuO boundary.

As for the side surface, where the oxidation takes place, the distribution of the copper atoms along the nanowire surface is:

$$D_{Cus0}exp\left(-\frac{e\varepsilon_{c2s}}{k_BT_s}\right)\frac{\partial^2 n_{cu}(z)}{\partial z^2} = -n_{Cu}(z)\frac{n_{x2s}}{n_0}\nu_0 exp\left(-\frac{e\varepsilon_{x-dis}}{k_BT_s}\right), \quad (S22)$$

$$\frac{\partial^2 n_{cu}(z)}{\partial z^2} = -n_{Cu}(z)\frac{n_{x2s}}{n_0}\frac{\nu_0}{D_{Cus0}}exp\left(-\frac{e(\varepsilon_{x-dis}-\varepsilon_{c2s})}{k_BT_s}\right), \quad (S23)$$

where n_{x2s} is the number density of oxygen molecules adsorbed on the side surface of a nanowire, and ε_{c2s} is the energy of dissociation in reaction (S3).

For $n_{Cu}(0) = n_{Cu20nw}$ the solution is

$$n_{Cu}(z) = n_{Cu20nw}cos\left[\left(\frac{n_{x2s}}{n_0}\frac{\nu_0}{D_{Cus0}}exp\left[-\frac{e(\varepsilon_{x-dis}-\varepsilon_{c2s})}{k_BT_s}\right]\right)^{1/2}z\right]. \quad (S24)$$

A rate of conversion (s^{-1}) of Cu atoms from Cu_2O to CuO on the side surface of a nanowire is:

$$N_{Cus}(L_{nw}) = \int_0^{L_{nw}} n_{Cu}(z)\frac{n_{x2s}}{n_0}\nu_0 exp\left(-\frac{e\varepsilon_{x-dis}}{k_BT_s}\right)2\pi R_{nw}(z)dz =$$

$$= n_{Cu20nw}\frac{n_{x2s}}{n_0}\nu_0 exp\left(-\frac{e\varepsilon_{x-dis}}{k_BT_s}\right)2\pi\int_0^{L_{nw}} R_{nw}(z)cos\left[\left(\frac{n_{x2s}}{n_0}\frac{\nu_0}{D_{Cus0}}exp\left[-\frac{e(\varepsilon_{x-dis}-\varepsilon_{c2s})}{k_BT_s}\right]\right)^{1/2}z\right]dz. \quad (S25)$$

Since a nanowire radius usually changes weakly along the nanowire, the following assumption $R_{nw}(0) \approx R_{nw}(L_{nw})$ can be used to simplify the expression:

$$N_{Cus}(L_{nw}) = 2\pi R_{nw}(0)\frac{\frac{n_{x2s}}{n_0}\nu_0 exp\left(-\frac{e\varepsilon_{x-dis}}{k_BT_s}\right)}{\left(\frac{n_{x2s}}{n_0}\frac{\nu_0}{D_{Cus0}}exp\left[-\frac{e(\varepsilon_{x-dis}-\varepsilon_{c2s})}{k_BT_s}\right]\right)^{1/2}}\times$$

$$\times\, n_{Cu20nw}sin\left[\left(\frac{n_{x2s}}{n_0}\frac{\nu_0}{D_{Cus0}}exp\left[-\frac{e(\varepsilon_{x-dis}-\varepsilon_{c2s})}{k_BT_s}\right]\right)^{1/2}L_{nw}\right]. \quad (S26)$$

As for the reactions on the nanowire tip, the rate of the conversion by the tip of a nanowire with the length L_{nw} is:

$$N_{Cut}(L_{nw}) = n_{Cu}(L_{nw})\frac{n_{x2t}}{n_0}\nu_0 exp\left(-\frac{e\varepsilon_{x-dis}}{k_BT_s}\right)\pi R_{nw}^2(L_{nw}) =$$

$$= \pi R_{nw}^2(L_{nw})\frac{n_{x2t}}{n_0}\nu_0 exp\left(-\frac{e\varepsilon_{x-dis}}{k_BT_s}\right)n_{Cu20nw}cos\left[\left(\frac{n_{x2s}}{n_0}\frac{\nu_0}{D_{Cus0}}exp\left[-\frac{e(\varepsilon_{x-dis}-\varepsilon_{c2s})}{k_BT_s}\right]\right)^{1/2}L_{nw}\right], \quad (S27)$$

where n_{x2t} is the density of O_2 molecules adsorbed on the tip.

The flux of Cu atoms consumed by a nanowire is

$$\varphi_{Cu2nw}(L_{nw}) = \frac{1}{\pi R_{nw}^2(0)}[N_{Cus}(L_{nw}) + N_{Cut}(L_{nw})]. \quad (S28)$$

By use of the assumption $R_{nw}(0) \approx R_{nw}(L_{nw})$ the expression is simplified:

$$\varphi_{Cu2nw}(L_{nw}) = n_{Cu20nw}\frac{n_{x2s}}{n_0}\nu_0 exp\left(-\frac{e\varepsilon_{x-dis}}{k_BT_s}\right)F(L_{nw}), \quad (S29)$$

$$F(L_{nw}) = \left[\begin{array}{c}\frac{2\left(\frac{n_{x2s}}{n_0}\frac{\nu_0}{D_{Cus0}}exp\left[-\frac{e(\varepsilon_{x-dis}-\varepsilon_{c2s})}{k_BT_s}\right]\right)^{-1/2}}{R_{nw}(0)}sin\left[\left(\frac{n_{x2s}}{n_0}\frac{\nu_0}{D_{Cus0}}exp\left[-\frac{e(\varepsilon_{x-dis}-\varepsilon_{c2s})}{k_BT_s}\right]\right)^{1/2}L_{nw}\right]+ \\ +\frac{n_{x2t}}{n_{x2s}}cos\left[\left(\frac{n_{x2s}}{n_0}\frac{\nu_0}{D_{Cus0}}exp\left[-\frac{e(\varepsilon_{x-dis}-\varepsilon_{c2s})}{k_BT_s}\right]\right)^{1/2}L_{nw}\right]\end{array}\right] \quad (S30)$$

Combination of (S21) and (S29) results in:

$$\varphi_{Cu2nw}(L_{nw}) = \frac{n_{x2s}\nu_0 exp\left(-\frac{e\varepsilon_{x-dis}}{k_BT_s}\right)F(L_{nw})}{1+\frac{a_0\nu_0}{D_{0c2}}L_{ox2}\frac{n_{x2s}}{n_0}exp\left[-\frac{e(\varepsilon_{x-dis}-\varepsilon_{c2})}{k_BT_s}\right]F(L_{nw})}, \quad (S31)$$

and after substitution (S31) to (S21):

$$n_{Cu20nw}(L_{ox2}) = \frac{n_0}{1+2\frac{a_0\nu_0}{2D_{0c2}}L_{ox2}\gamma_L F(L_{nw})}, \quad \text{(S32)}$$

At a time t the nanowires grown per unit of area consume the flux:

$$\varphi_{Cu2n}(t) = \int_0^{L_{nw-m}} \rho_D(L)\varphi_{Cu2nw}(L)dL = \int_0^{L_{nw-m}} \rho_D(L)\frac{n_{x2s}\nu_0 exp\left(-\frac{e\varepsilon_{x-dis}}{k_B T_s}\right)F(L)}{1+\frac{a_0\nu_0}{D_{0c2}}L_{ox2}\frac{n_{x2s}}{n_0}exp\left[-\frac{e(\varepsilon_{x-dis}-\varepsilon_{c2})}{k_B T_s}\right]F(L)}dL, \quad \text{(S33)}$$

where $\rho_D(L)$ is the density of distribution of the nanowires on length.

Finally, two expressions can be obtained for the rate of the nanowire growth in length

$$\frac{dL_{nw}}{dt}(L_{nw}) = N_{Cut}(L_{nw})\frac{a_0^3}{\pi R_{nw}^2(L_{nw})} =$$

$$= n_{Cu20nw}(L_{nw})cos\left[\left(\frac{n_{x2s}}{n_0}\frac{\nu_0}{D_{Cus0}}exp\left[-\frac{e(\varepsilon_{x-dis}-\varepsilon_{c2s})}{k_B T_s}\right]\right)^{1/2}L_{nw}\right]\frac{n_{x2t}}{n_0}\nu_0 exp\left(-\frac{e\varepsilon_{x-dis}}{k_B T_s}\right)a_0^3, \quad \text{(S34)}$$

and the rate of growth of nanowire radius

$$\frac{dR_{nw}}{dt}(z,t,L_{nw}) = n_{Cu}(z)\frac{n_{x2s}}{n_0}\nu_0 exp\left(-\frac{e\varepsilon_{x-dis}}{k_B T_s}\right)a_0^3 =$$

$$= n_{Cu20nw}(L_{nw})\frac{n_{x2s}}{n_0}\nu_0 exp\left(-\frac{e\varepsilon_{x-dis}}{k_B T_s}\right)a_0^3 cos\left[\left(\frac{n_{x2s}}{n_0}\frac{\nu_0}{D_{Cus0}}exp\left[-\frac{e(\varepsilon_{x-dis}-\varepsilon_{c2s})}{k_B T_s}\right]\right)^{1/2}z\right]. \quad \text{(S35)}$$

In the case of application of the stage of intermediate deposition the schematic of the nanowire growth is shown in **Scheme S3**.

The stage of the intermediate deposition results in changing the number of adsorption nodes, which could be occupied by oxygen molecules, because the deposited atoms of noble metal occupy a part of the nanowire surface yet do not serve as adsorption nodes for oxygen. This fact is reflected by introducing the additional conditions:

$$\frac{n_{x2s}(t)}{n_0} = \begin{cases} \frac{P_{O2}}{P_{0s}+P_{O2}}, & t < t_{dep} \\ \alpha_{nx}\frac{P_{O2}}{P_{0s}+P_{O2}}, & t \geq t_{dep} \end{cases}, \quad \text{(S36)}$$

$$\frac{n_{x2t}(t)}{n_0} = \begin{cases} \frac{P_{O2}}{P_{0s}+P_{O2}}, & t < t_{dep} \\ \alpha_{nxt}\frac{P_{O2}}{P_{0s}+P_{O2}}, & t \geq t_{dep} \end{cases} \quad \text{(S37)}$$

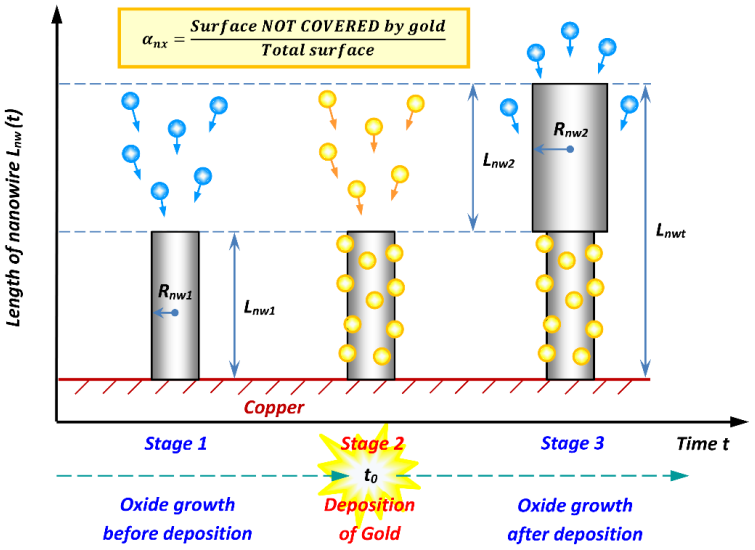

Scheme S3. A schematic of changing a morphology of a nanowire in a case when the maximum length of the nanowire is achieved before the stage of the intermediate deposition of gold: t_0 is a time when the discharge is powered off, and gold nanoparticles are deposited on a surface of a nanowire (time of the deposition of gold is not considered); L_{nw1} is a length of the nanowire at the moment t_0; R_{nw1} is a radius of the nanowire at the moment t_0; L_{nw2} is a length of a part of the nanowire grown after at the moment t_0 (gold is deposited on the part L_{nw1}, while the part L_{nw2} is considered as gold-free); R_{nw12} is a radius of the part L_{nw1} of the nanowire grown after t_0; R_{nw2} is a radius of the part L_{nw2} of the nanowire grown after t_0; L_{nwt} is a total length of the nanowire after the treatment

where t_{dep} is the time when the deposited metal is considered as acting on the side and top surfaces of a nanowire; α_{nx} and α_{nxt} are the coefficient less than unity, which describe the parts of the side and top NW surfaces that are non-covered by the noble metal, respectively.

Finally, a system of the equations is set:

$$\frac{dL_{ox1}}{dt} = \begin{cases} \left(\frac{P_{b1}}{1+a_{b1}L_{ox1min}} + \frac{P_{l1}}{1+a_{l1}L_{ox1min}}\right)A_c, & (L_{ox1}(t) \le L_{ox1min}) \wedge (L_{ox2}(t) \le L_{ox2min}) \\ \left(\frac{P_{b1}}{1+a_{b1}L_{ox1}} + \frac{P_{l1}}{1+a_{l1}L_{ox1}}\right)A_c - \left(\frac{2B_c}{1+bL_{ox2min}} + \frac{2C_c}{1+cL_{ox2min}}\right) - D_{nw}\frac{a_{ox1}^3}{a_{ox2}^3}D_c(L_{ox2min}), & (L_{ox1}(t) > L_{ox1min}) \wedge (L_{ox2}(t) \le L_{ox2min}) \\ \left(\frac{P_{b1}}{1+a_{b1}L_{ox1}} + \frac{P_{l1}}{1+a_{l1}L_{ox1}}\right)2A_c - \left(\frac{2B_c}{1+bL_{ox2}} + \frac{2C_c}{1+cL_{ox2}}\right) - D_{nw}\frac{a_{ox1}^3}{a_{ox2}^3}D_c(L_{ox2}), & (L_{ox1}(t) > L_{ox1min}) \wedge (L_{ox2}(t) > L_{ox2min}) \\ \left(\frac{P_{b1}}{1+a_{b1}L_{ox1min}} + \frac{P_{l1}}{1+a_{l1}L_{ox1min}}\right)2A_c, & (L_{ox1}(t) \le L_{ox1min}) \wedge (L_{ox2}(t) > L_{ox2min}) \\ 0, \quad \text{otherwise} \end{cases} \tag{S38}$$

$$\frac{dL_{ox2}}{dt} = \begin{cases} \left(\frac{2B_c}{1+bL_{ox2min}} + \frac{2C_c}{1+cL_{ox2min}}\right), & (L_{ox1}(t) > L_{ox1min}) \wedge (L_{ox2}(t) \le L_{ox2min}) \\ -\left(\frac{P_{b1}}{1+a_{b1}L_{ox1}} + \frac{P_{l1}}{1+a_{l1}L_{ox1}}\right)A_c + \left(\frac{2B_c}{1+bL_{ox2}} + \frac{2C_c}{1+cL_{ox2}}\right), & (L_{ox1}(t) > L_{ox1min}) \wedge (L_{ox2}(t) > L_{ox2min}) \\ -\left(\frac{P_{b1}}{1+a_{b1}L_{ox1min}} + \frac{P_{l1}}{1+a_{l1}L_{ox1min}}\right)A_c, & (L_{ox1}(t) \le L_{ox1min}) \wedge (L_{ox2}(t) > L_{ox2min}) \\ 0, \quad \text{otherwise} \end{cases} \tag{S39}$$

$$\frac{dL_{ox}}{dt} = \begin{cases} \left(\frac{P_{b1}}{1+a_{b1}L_{ox1min}} + \frac{P_{l1}}{1+a_{l1}L_{ox1min}}\right)A_c, & (L_{ox1}(t) \le L_{ox1min}) \wedge (L_{ox2}(t) \le L_{ox2min}) \\ \left(\frac{P_{b1}}{1+a_{b1}L_{ox1}} + \frac{P_{l1}}{1+a_{l1}L_{ox1}}\right)A_c - D_{nw}\frac{a_{ox1}^3}{a_{ox2}^3}D_c(L_{ox2min}), & (L_{ox1}(t) > L_{ox1min}) \wedge (L_{ox2}(t) \le L_{ox2min}) \\ \left(\frac{P_{b1}}{1+a_{b1}L_{ox1}} + \frac{P_{l1}}{1+a_{l1}L_{ox1}}\right)A_c - D_{nw}\frac{a_{ox1}^3}{a_{ox2}^3}D_c(L_{ox2}), & (L_{ox1}(t) > L_{ox1min}) \wedge (L_{ox2}(t) > L_{ox2min}) \\ \left(\frac{P_{b1}}{1+a_{b1}L_{ox1min}} + \frac{P_{l1}}{1+a_{l1}L_{ox1min}}\right)A_c, & (L_{ox1}(t) \le L_{ox1min}) \wedge (L_{ox2}(t) > L_{ox2min}) \\ 0, \quad \text{otherwise} \end{cases} \tag{S40}$$

$$\frac{dR_{nw}}{dt} = \begin{cases} \alpha_L(t)\frac{n_{x2s}(t)}{n_{x2t}(t)}n_{Cu20nw}(L_{ox2min}), & (L_{ox1}(t) > L_{ox1min}) \wedge (L_{ox2}(t) \le L_{ox2min}) \\ \alpha_L(t)\frac{n_{x2s}(t)}{n_{x2t}(t)}n_{Cu20nw}(L_{ox2}), & (L_{ox1}(t) > L_{ox1min}) \wedge (L_{ox2}(t) > L_{ox2min}) \\ 0, \quad \text{otherwise} \end{cases} \tag{S41}$$

$$\frac{dL_{nw}}{dt} = \begin{cases} \alpha_L(t)n_{Cu20nw}(L_{ox2min})cos(\beta_L L_{nw}), & (L_{ox1}(t) > L_{ox1min}) \wedge (L_{ox2}(t) \le L_{ox2min}) \\ \alpha_L(t)n_{Cu20nw}(L_{ox2})cos(\beta_L L_{nw}), & (L_{ox1}(t) > L_{ox1min}) \wedge (L_{ox2}(t) > L_{ox2min}) \\ 0, \quad \text{otherwise} \end{cases} \tag{S42}$$

with the following initial conditions: $L_{ox1}(0) = L_{10}$, $L_{ox2}(0) = L_{20}$, $L_{ox}(0) = L_{10} + L_{20}$.

The parameters used in the system are:

$$A_c = n_{CuO}a_0^3\frac{\nu_0}{2}; \qquad B_c = 2n_{x0}a_0^3\frac{\nu_0}{2}exp\left(-\frac{e(\varepsilon_{x2}+\varepsilon_{x-dec})}{k_BT_s}\right); \quad C_c = n_{x0}a_0^3\frac{\nu_0}{2}exp\left(-\frac{e(\varepsilon_{c2}+\varepsilon_{x-dec})}{k_BT_s}\right); \tag{s43}$$

$$D_c(L_i) = n_{Cu20nw}(L_i)\pi R_{nw}^2(L_{nw})\alpha_L(t)cos(\beta_L(t)L_{nw}) + 2\pi R_{nw}(0)\frac{n_{x2s}(t)}{n_{x2t}(t)}\frac{\alpha_L(t)}{\beta_L(t)}sin(\beta_L(t)L_{nw}); \tag{s44}$$

$$P_{b1} = \frac{1}{\left(1+\frac{d_{Cu20}}{2b_{Cu20}}\right)}exp\left[-\frac{e\varepsilon_{c1b}}{k_BT_s}\right]; \qquad P_{l1} = \frac{1}{\left(1+\frac{2b_{Cu20}}{d_{Cu20}}\right)}exp\left[-\frac{e\varepsilon_{c1l}}{k_BT_s}\right]; \tag{s45}$$

$$a_{b1} = \frac{a_0\nu_0}{2D_{0c1b}}; \qquad a_{l1} = \frac{a_0\nu_0}{2D_{0c1l}}; \qquad b = \frac{a_0\nu_0}{2D_{0x2}}; \qquad c = \frac{a_0\nu_0}{2D_{0c2}}; \tag{s46}$$

$$\frac{n_{x2s}(t)}{n_0} = \begin{cases} \frac{P_{O2}}{P_{0s}+P_{O2}}, & t < t_{dep} \\ \alpha_{nx}\frac{P_{O2}}{P_{0s}+P_{O2}}, & t \ge t_{dep} \end{cases}; \qquad \frac{n_{x2t}(t)}{n_0} = \begin{cases} \frac{P_{O2}}{P_{0s}+P_{O2}}, & t < t_{dep} \\ \alpha_{nxt}\frac{P_{O2}}{P_{0s}+P_{O2}}, & t \ge t_{dep} \end{cases}; \tag{s47}$$

$$\alpha_L(t) = \frac{n_{x2t}(t)}{n_0}a_{0s}^3\nu_0 exp\left(-\frac{e\varepsilon_{x-dis}}{k_BT_s}\right); \qquad \beta_L(t) = \left(\frac{n_{x2s}(t)}{n_0}\frac{\nu_0}{D_{Cus0}}exp\left[-\frac{e(\varepsilon_{x-dis}-\varepsilon_{c2s})}{k_BT_s}\right]\right)^{1/2}; \tag{s48}$$

$$\gamma_L(t) = \frac{n_{x2s}(t)}{n_{0s}} exp\left[-\frac{e(\varepsilon_{x-dis}-\varepsilon_{c2})}{k_B T_s}\right]; \qquad n_{Cu20nw}(L_i) = \frac{n_0}{1+2cL_i\gamma_L F(L_{nw})}; \tag{s49}$$

$$F(L_{nw}) = \frac{2}{\beta_L R_{nw}(0)} sin(\beta_L(t)L_{nw}) + \frac{n_{x2t}}{n_{x2s}} cos(\beta_L(t)L_{nw}). \tag{s50}$$

2. Details of simulation

The model simulated the growth of CuO nanowires at the fixed conditions described in the experimental section. Thus, the oxygen partial pressure was set to $2.1 \cdot 10^4$ Pa, and the experimental dependence of the sample temperature is approximated by the expression: $T_s(t) = (T_{max} - T_0)(1 - exp[-t/\tau]) + 293$ (K), where T_{max} = 315 °C; T_0 = 20 °C, τ = 40 s.

The adsorption energy ε_{aO2} = 1.46 eV on a surface of CuO oxide was set to fit the experimental data and is higher than the value of 1.35 eV perfect calculated by Sun *et al*. [4] for the adsorption of O_2 on the perfect and oxygen-deficient CuO surface with vacancies. This difference can be explained by the higher disorder in crystallinity of the real oxide. The energy ε_{aO2nws} = 0.1 eV of oxygen adsorption of side surface of a nanowire corresponds to the lowest energy of O_2 adsorbed on the perfect and oxygen-deficient CuO (111) surface [4], where the adsorption energies of the modes O_2 being perpendicular to the I, III, IV, V, VI, VII and VIII sites are between 0.1–0.18 eV. At the same time, the energy ε_{aO2nwt} = 0.385 eV is located in the range between the energy of 0.32 eV that is calculated for the O_2 adsorbed on the II site ($O_{2(a)}$ mode), and the energy of 0.45 eV that fits to $O_{2(b)}$ mode [4]; both of the modes correspond to the adsorption of O_2 on the perfect CuO (111) surface. It should be mentioned that Hu *et al.* also pointed that the attraction between O_2 and CuO (111) is weak; according to their data the binding energy is 0.27 eV per O_2 molecule [5].

3. Additional simulation results

The value of the dissociation energy of O_2 on the Cu_2O surface $\varepsilon_{x\text{-}dis}$ = 0.65 eV is close to the value of 0.85 eV for O_2 dissociation on the Cu_2O (111) surface (M(d)→P3 reaction) and is higher that the energy of 0.18 eV (M(e)→P4 reaction) that were calculated by Zhang *et al.* for O_2 dissociation on the Cu_2O oxygen-deficient surface [6].

The energies ε_{c1b} = 0.98 eV and ε_{c1l} = 1.5 eV of the boundary and lattice diffusion of copper atoms through Cu_2O layer were set to correspond the reported data [2,7] and to fit the results on the measured thicknesses of Cu_2O and CuO oxides.

The energy ε_{x2} = 0.8 eV of O_2 diffusion through CuO layer is engaged to describe the growth of CuO layer not only in this experiment, but also the results obtained by Zhu *et al.* and Yuan *et al.* in their experiments [8,9]. The energies ε_{c2} = 0.66 eV and ε_{c2s} = 0.46 eV (or 0.56 eV) of Cu diffusion in the CuO layer and along the side surface of CuO nanowire toward its tip were set to fit the ratio of thicknesses of both oxides to the data from the experiments. The internal energy ε_{iO2} = 0.31 eV of oxygen molecules adsorbed on surfaces of oxide layer and nanowires, is used to fit the experimental data within the frame of the developed model.

The results of 3D modelling are shown in **Figure S1**, which clearly indicates the effectiveness of the proposed approach.

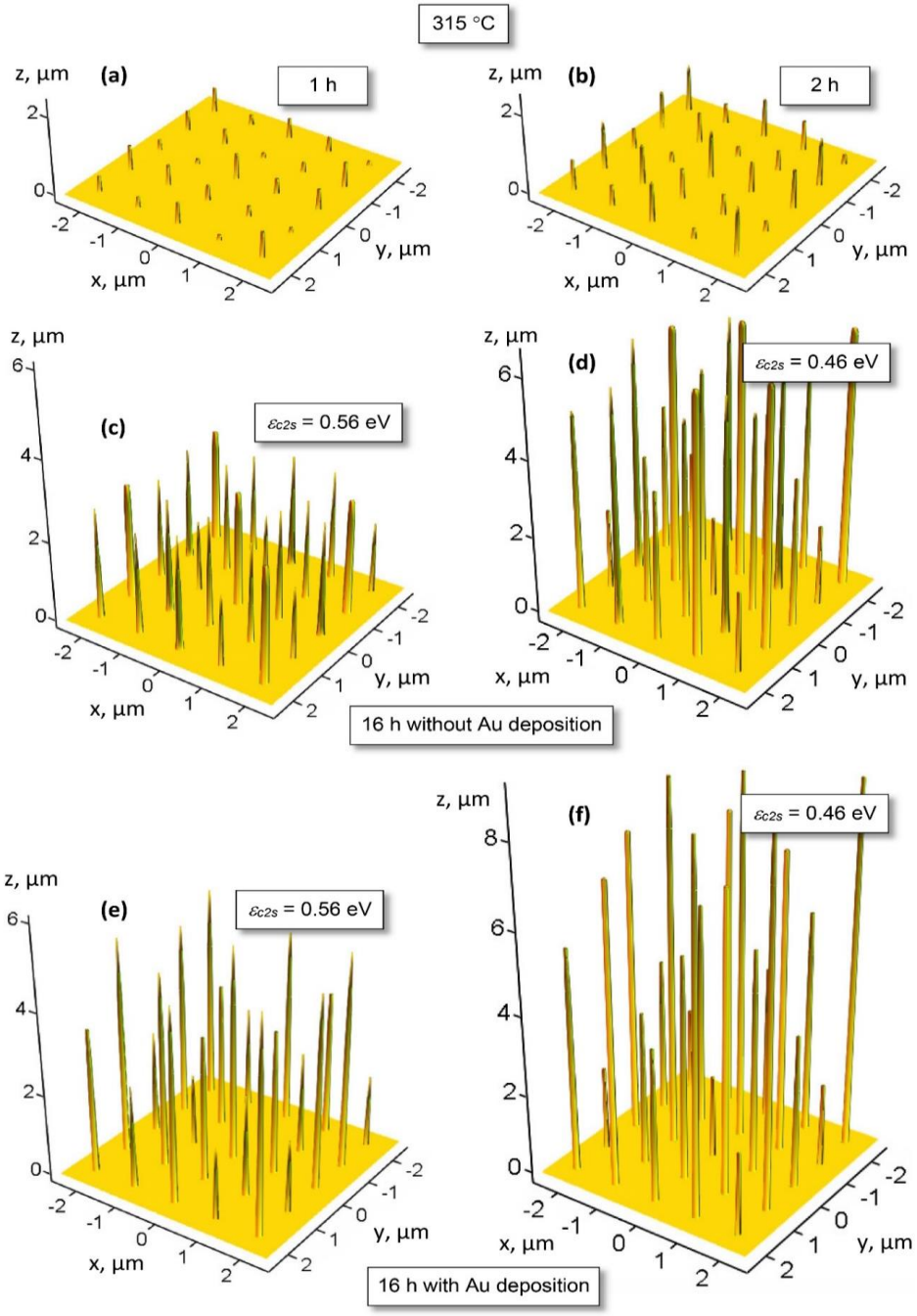

Figure S1. Growth of copper oxide nanowires at the dependence on the activation energy ε_{c2s} of copper diffusion along the surface of the nanowire; gold deposition was realized after 8 hours of nanowire growth (Fig. 6): a – one hour of growth, b – two hours; c, d – 16 hours without gold deposition: c – ε_{c2s} = 0.56 eV; d – ε_{c2s} = 0.46 eV; d, e – 16 hours of growth under condition of the deposition of gold at the eighth hour of growth: e – ε_{c2s} = 0.56 eV; f – ε_{c2s} = 0.46 eV.

4. Description of the experiment

The reactor was made of a fused silica tube passing through a resonant cavity connected to a microwave generator operating at 2.45 GHz and 100 W of applied power. During the plasma source operation, Ar - 10 vol.% O_2 plasma at atmospheric pressure is forced to stay on the tube axis by a rotating fan. Neutral species that are not subjected to the influence of the electric field exit the reactor through an orifice of 400 µm in diameter. A total flow rate of 275 sccm (standard cubic centimetre per minute) is injected in

the plasma, which produces a laminar post-discharge (**Figure S2b**), containing atomic oxygen and various neutral excited species of oxygen like the singlet state of O_2. The beam diameter is nearly twice the diameter of the hole (~ 800 µm). Under these experimental conditions, the gas temperature is ~1200 K and high thermal gradients exist. The evolution of the surface temperature of the substrate was determined by heat transfer simulation from time-resolved infrared measurements on the sample backside. The surface temperature reaches a steady state after about 3 minutes and the maximum temperature lies in the range [280 – 350 °C], depending on the experimental conditions. The hole-substrate distance is 2 mm and the treatment is performed in a confined environment to prevent air contamination. **Figure S2** shows a copper thin film after afterglow oxidation. Coloured rings appear on the substrate area hit by the afterglow over a diameter comprised between 1 and 2 centimetres.

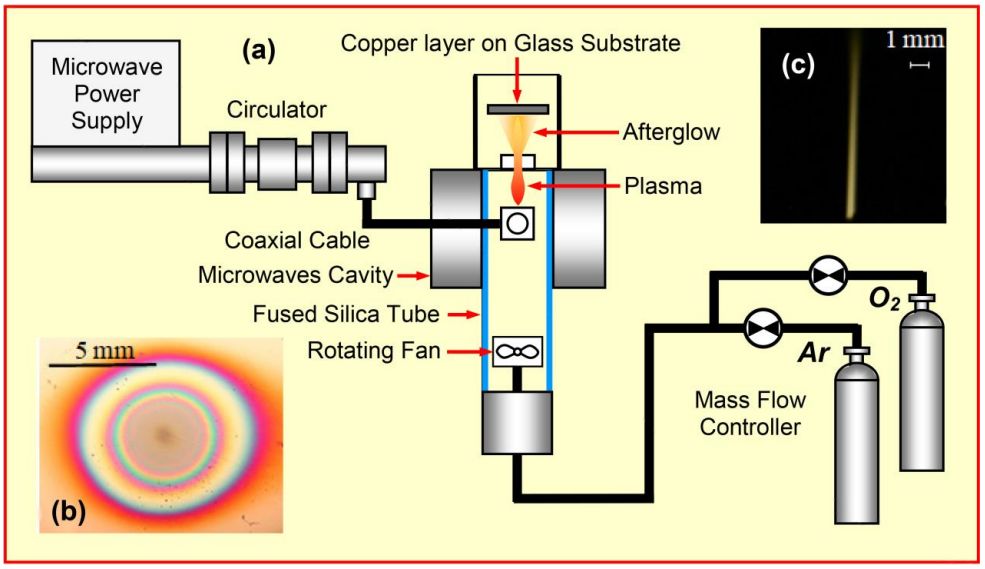

Figure S2. Schematic of the experimental setup (a), photograph of copper thin film after two-hour afterglow oxidation (b), and photograph of the micro-afterglow through a 400-µm diameter orifice (c).

5. Experimental results

To follow the growth of nanowires during synthesis, gold particles were used. The synthesis process was divided into 2 steps of one hour each, under the conditions described previously (Ar - 10 vol.% O_2, 275 Nccm, 100 W). Under these conditions, a one hour-long treatment led to the formation of relatively long nanowires: around 600 nm in the optimal growth zone. After this first step, the sample was covered by gold in a metallizer (Denton Vacuum Desk IV). The duration of the deposit was short enough for the gold to form separated nanoparticles on the surface of the sample.

Gold was chosen because of its non-oxidizable nature. After gold deposit, the sample underwent a second oxidation treatment for one hour under the same conditions. The obtained nanowires were characterized by transmission electron microscopy (TEM). It can be seen in the general view (Figure S3) that the lengths of the nanowires are between 1 and 1.5 µm. A large number of nanoparticles with diameters between 2 and 5 nm are observed at the base of the nanowires (Figure S3b).

On the other hand, no nanoparticle was visible at the top of the wires (Figure S3c). To confirm these observations, high resolution images were taken respectively at the top (Figure S3d) and at the base of the nanowires (Figure S3e,f). The crystal structure of the upper part of the nanowire is comparable to observations made on the nanowires without gold deposits. In particular, in the upper part of the image, the spacing between two consecutive planes is 0.25 nm, which is compatible with the lattice parameter of the (-111) plane of the monoclinic phase of CuO. Other interplanar spacings of approximately 0.23 and

0.20 nm are measured observed at the base of the nanowires, especially in the nanoparticles. These spacings correspond respectively to the (111) and (200) planes of the face centered cubic phase of gold (JCPDS 03-065-2870) but also to the (111) and (11-2) planes of CuO.

To fully determine the nature of the nanoparticles, energy dispersion spectra (EDS) were acquired respectively in the middle (Figure S4a) and at the base of the nanowires (Figure S4b). These spectra clearly show the presence of gold at the base of the nanowires. No trace of gold is visible at the top of the nanowires. In addition, a random analysis of the nanowires in the sample confirmed that the nanoparticles are only present in the lower part, approximately between the base (at the interfacial zone between the film and the wires) and the middle of the nanowire.

These observations show that nanowires continued growing during the second oxidation stage without affecting the position of the gold nanoparticles. These results confirm that the growth of nanowires is not affected by the base of the wire but by diffusion of copper ions towards the top. In addition, nanoparticles seem to be present on the surface of nanowires. However, the diameters of the nanowires increase weakly between 1 and 2 hours of treatment under these experimental conditions: on average between 55 and 60 nm. These experiments therefore do not allow a decision to be made between surface and volume diffusion mechanisms.

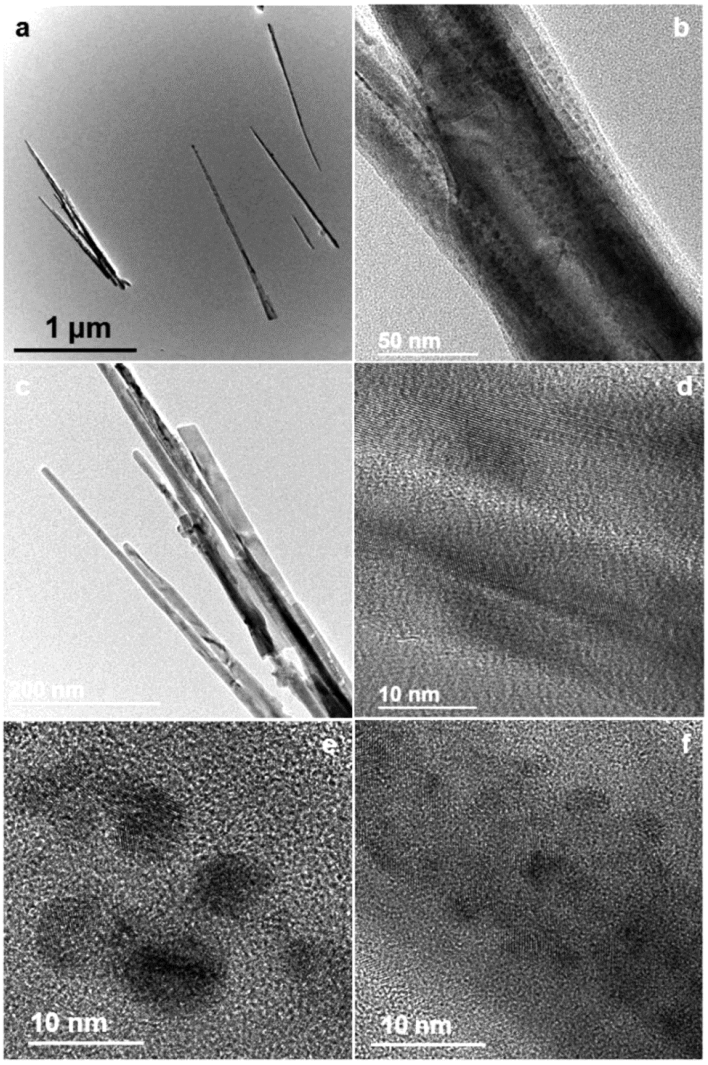

Figure S3. Electron microscopy of CuO nanowire: (a) General overview of CuO nanowires after the deposition of Au nanoparticles and two-step oxidation process; (b) Base and (c) top of the nanowires; High resolution of top (d) and base (e and f) of the nanowires.

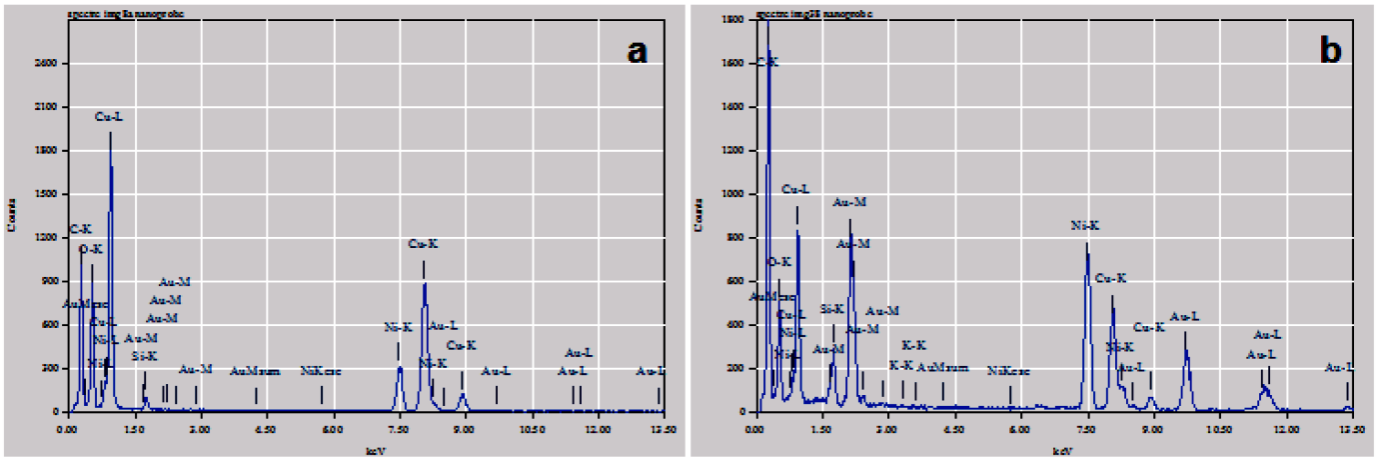

Figure S4. EDX measurements at the top (a) ant base (b) of a nanowire.

References

[1] C. Kittel, and H. Kroemer, Thermal Physics, W. H. Freeman and Co, New York, 1980.

[2] Y. Zhu, K. Mimura, J.-W. Lim, M. Isshiki, Q. Jiang, Brief Review of Oxidation Kinetics of Copper at 350 °C to 1050 °C. *Metall. and Mat. Trans. A* **2006**, *37*, 1231–1237.

[3] I. Levchenko, U. Cvelbar, M. Keidar, Graphene Flakes in Arc Plasma: Conditions for the Fast Single-Layer Growth, Graphene 5 (2016), 81–89, http://dx.doi.org/10.4236/graphene.2016.52009

[4] S. Sun, C. Li, D. Zhang, Y. Wang, Density functional theory study of the adsorption and dissociation ofO2on CuO(1 1 1) surface, Applied Surface Science 333 (2015) 229–234, https://doi.org/10.1016/j.apsusc.2015.02.018

[5] J. Hu, D. Li,| J. G. Lu, R. Wu, Effects on Electronic Properties of Molecule Adsorption on CuO Surfaces and Nanowires, The Journal of Physical Chemistry C 114 (2010) 17120–17126, https://pubs.acs.org/doi/pdf/10.1021/jp1039089

[6] R. Zhang, H. Liu, H. Zheng, L. Ling, Z. Li, B. Wang, Adsorption and dissociation of O2 on the Cu2O(1 1 1) surface: Thermochemistry, reaction barrier, Applied Surface Science 257 (2011) 4787–4794, https://doi.org/10.1016/j.apsusc.2010.12.040

[7] N. L. Peterson, C. L. Wiley, Diffusion and Point Defects in Cu2O. *J. Phys. Chem. Solids* **1984**, *45 (3)*, 281–294.

[8] L. Yuan, Y. Wang, R. Mema, G. Zhou, Driving force and growth mechanism for spontaneous oxide nanowire formation during the thermal oxidation of metals, Acta Mater. 59 (2011) 2491–2500. https://doi.org/10.1016/j.actamat.2010.12.052

[9] Y. Zhu, K. Mimura, M. Isshiki, Oxidation Mechanism of Copper at 623–1073 K, Materials Transactions 43 (9) (2002) 2173–2176, https://doi.org/10.2320/matertrans.43.2173